1
2
3

Molecular basis for shifted receptor recognition by an encephalitic arbovirus

4   Xiaoyi Fan[1,#], Wanyu Li[1,#], Jessica Oros[1], Jesse S. Plung[1], Jessica A. Plante[2,3,4], Himanish Basu[5],
5   Sivapratha Nagappan-Chettiar[6], Joshua M. Boeckers[6], Laurentia V. Tjang[1], Colin J. Mann[1],
6   Vesna Brusic[1], Tierra K. Buck[1], Haley Varnum[1], Pan Yang[1], Linzy M. Malcolm[1], So Yoen Choi[5],
7   William M. de Souza[7], Isaac M. Chiu[5], Hisashi Umemori[6], Scott C. Weaver[2,3,4], Kenneth S.
8   Plante[2,3,4], Jonathan Abraham[1,8,9,10,*]
9

10   [1]Department of Microbiology, Blavatnik Institute, Harvard Medical School, Boston, MA, USA
11   [2]World Reference Center for Emerging Viruses and Arboviruses, University of Texas Medical
12   Branch, Galveston, TX, USA
13   [3]Department of Microbiology and Immunology, University of Texas Medical Branch, Galveston,
14   TX, USA
15   [4]Institute for Human Infections and Immunity, University of Texas Medical Branch, Galveston, TX,
16   USA
17   [5]Department of Immunology, Blavatnik Institute, Harvard Medical School, Boston, MA, USA
18   [6]Department of Neurology, F.M. Kirby Neurobiology Center, Boston Children's Hospital, Harvard
19   Medical School, Boston, MA, USA
20   [7]Department of Microbiology, Immunology, and Molecular Genetics, University of Kentucky
21   College of Medicine, KY, USA
22   [8]Department of Medicine, Division of Infectious Diseases, Brigham & Women's Hospital, Boston,
23   MA, USA
24   [9]Center for Integrated Solutions in Infectious Diseases, Broad Institute of Harvard and MIT,
25   Cambridge, MA, USA
26   [10]Howard Hughes Medical Institute, Boston, MA, USA
27   [#]These authors contributed equally
28
29   [*]Correspondence: jonathan_abraham@hms.harvard.edu (J.A.)
30

Abstract

After decades of inactivity throughout the Americas, western equine encephalitis virus (WEEV) recently re-emerged in South America, causing a large-scale outbreak in humans and horses. WEEV binds protocadherin 10 (PCDH10) as a receptor; however, nonpathogenic strains no longer bind human or equine PCDH10 but retain the ability to bind avian receptors. Highly virulent WEEV strains can also bind the very low-density lipoprotein receptor (VLDLR) and apolipoprotein E receptor 2 (ApoER2) as alternative receptors. Here, by determining cryo-electron microscopy structures of WEEV strains isolated from 1941–2005 bound to mammalian receptors, we identify polymorphisms in the WEEV spike protein that explain shifts in receptor dependencies and that can allow nonpathogenic strains to infect primary cortical neurons. We predict the receptor dependencies of additional strains and of a related North American alphavirus. Our findings have implications for outbreak preparedness and enhance understanding of arbovirus neurovirulence through virus receptor binding patterns.

Introduction

Several alphaviruses cause outbreaks of encephalitis in humans and equids with unpredictable frequency and scale. These include western equine encephalitis virus (WEEV), eastern equine encephalitis virus (EEEV), and Venezuelan equine encephalitis virus (VEEV).[1-3] Manifestations of WEEV infection range from mild or asymptomatic illness to encephalitis, and survivors can be left with devastating neurological sequalae that include seizures and cognitive impairment.[3] WEEV previously caused large outbreaks of encephalitis in horses and humans in the early 20th century in North America, but outbreaks have since drastically decreased in both frequency and scale (a phenomenon known as viral "submergence").[4] The last documented human case of WEEV in North America was in 1999, although the virus can still be detected in mosquito pools. Until very recently, the last outbreak of WEEV in South America was more than three decades ago,[5] with only sporadic spillover events observed thereafter. For example, there was a single fatal human case in Uruguay in 2009, even though the presence of WEEV in Uruguay had not been documented since the 1970s.[6] However, from November of 2023 to April of 2024, WEEV unexpectedly re-emerged in South America, causing a large-scale outbreak that involved over 2,500 equine cases, over 200 human cases, and resulted in a total of 12 human fatalities in Argentina, Uruguay, and Brazil.[7-9]

WEEV binds protocadherin 10 (PCDH10), a membrane protein that is broadly expressed but whose expression is particularly enriched in the brain, as a cellular receptor on mammalian cells.[10,11] PCDH10 is a non-clustered δ2 protocadherin that is involved in synapse development.[12,13] The PCDH10 ectodomain contains six extracellular cadherin repeats (EC1–6) that are connected by loops that are rigidified by calcium coordination (Figure 1A).[14] The WEEV spike protein binds PCDH10 EC1, which is the most membrane-distal repeat in the receptor ectodomain.[10,11] PCDH10 shares no structural homology with any previously described alphavirus receptors (e.g., matrix remodeling-associated protein 8 (MXRA8) or low-density lipoprotein

69   receptor (LDLR)-related proteins);[15-22] therefore, how PCDH10 interacts with alphavirus spike

70   proteins is unknown.

71   WEEV strains isolated in North America are divided into lineages A and B; lineage B is

72   further subdivided into B1, B2, and B3 (Figures 1B and S1; Table S1). Later lineages displaced

73   earlier ones, and B3 is the most recently detected sublineage in North America.[4] While human

74   PCDH10 is a general receptor for most WEEV strains we previously tested, lineage A strains,

75   which are highly virulent in animal models and were isolated in North America in the 1930s–

76   1940s, also bind VLDLR and ApoER2 (Figure 1B).[10,23] Imperial 181 is a B3 WEEV strain that was

77   isolated from a mosquito pool in California in 2005 and is nonpathogenic in animal models.[4,24]

78   Despite not binding to human or murine PCDH10,[10] Imperial 181 can still bind PCDH10 orthologs

79   of WEEV's enzootic hosts, which include house sparrows (*Passer domesticus*). Imperial 181 can

80   also bind the ortholog of common garter snakes (*Thamnophis sirtalis*), which are proposed

81   overwintering hosts.[10,25,26] The molecular basis for shifting patterns of receptor binding by different

82   WEEV strains isolated in North America over the past century is unknown, nor are the receptor-

83   binding properties of WEEV strains that recently re-emerged in South America.

84   Here, we conducted in depth structural and functional analyses of WEEV interactions with

85   its alternative cellular receptors to identify the spike protein polymorphisms that explain the

86   dynamic patterns of receptor recognition during the evolution of this important human pathogen.

87

88   **Results**

89   **Structure of WEEV bound to human PCDH10**

90   The alphavirus genome encodes four nonstructural proteins and structural proteins

91   capsid, E3, E2, 6K, TF, and E1.[2] The viral spike proteins E2 and E1 are arranged with icosahedral

92   symmetry on the surface of virions.[27-29] E2 and E1 form heterodimers that assemble as 80 trimers

93   that bind receptors and mediate the fusion of viral and cellular membranes during viral entry.[27-29]

94   For structural analysis, we produced WEEV CBA87 virus-like particles (VLPs) (Figure S2A). This

95   strain was previously isolated from the brain of an infected horse in Córdoba, Argentina, in 1958

96   and has been used in investigational VLP-based vaccines that were modified for high-yield

97   expression.[30] In biolayer interferometry experiments, monomeric soluble EC1 interacted with

98   immobilized WEEV CBA87 VLPs with a K_D of 5.6 µM (Figures S2A–E). This affinity is similar to

99   that of the PCDH10 ectodomain for itself during homodimerization (reported K_D of 3.6 µM).[14]

100   We determined cryo-EM structures of CBA87 VLPs alone or bound to PCDH10 EC1

101   (Figures 1C–E, S3A–F, and S4A). The resolutions of maps of the receptor-bound and unliganded

102   quasi-threefold (q3) spikes were 2.9 Å (masked spike protein trimer) and 3.4 Å (q3 block),

103   respectively (Table S2). In the receptor bound structure, PCDH10 EC1 is inserted into clefts

104   formed by adjacent E2–E1 protomers (Figure 1E). The angle of receptor binding is roughly 45

105   degrees in the long axis of EC1 with respect to the threefold axis of the spike protein trimer (Figure

106   1D). PCDH10 EC1 makes extensive contacts with E2 and E1 protomers on both sides of each

107   cleft and buries a large surface area (~1,500 Å^2) as it interacts with the WEEV spike protein

108   (Figure S5A). When structures of receptor-bound alphavirus spike proteins are compared, this

109   receptor contact surface is larger than those of alphavirus spike proteins with individual LDLR

110   class A (LA) repeats but smaller than those of human or avian MXRA8 (Figure S5A).[15-22] There is

111   no conformational change in the WEEV spike protein or in PCDH10 EC1 when structures of the

112   WEEV spike protein bound to EC1 or of EC1 as part of the EC1–EC4 homodimer are compared

113   (Figure S3G).[14]

114   One face of the cadherin repeat makes prominent contacts with the β-ribbon of E2 domain

115   A (Figure S5D). These contacts involve PCDH10 residues N40 and R42 and WEEV residues D40,

116   D156, and H157, which are in the central arch of the β-ribbon (Figure 1F). Additionally, PCDH10

117   residues P39, F80, L85, and L87 contact multiple E2 β-ribbon residues including L149, T262,

118   T264, and V265 (Figure 1G). The contralateral face of the cadherin repeat makes several contacts

119   with the adjacent E2–E1 protomer (E2'-E1') (Figure S5E). As part of these interactions, PCDH10

120   residues E21 and D22 make salt bridges with E2' domain B residues K177 and K224 (Figure 1H).

121   Additionally, PCDH10 residue H76 and E2 residue H21 are involved in stacking interactions

122   (Figure 1I). PCDH10 residues L2 and H3 contact E1' fusion loop residues F87 and W89 and

123   PCDH10 residue F88 contacts E1' residue K227 (Figure 1J). Other than the two E1' fusion loop

124   contact residues, the WEEV spike protein residues that contact PCDH10 are not conserved in

125   EEEV or VEEV, explaining why these other encephalitic alphaviruses do not bind PCDH10

126   (Figures S6A and S6B).[10]

127   Interestingly, the hydrophobic interactions the WEEV spike protein makes with human

128   PCDH10 resemble how PCDH10 EC1 interacts with EC4 during antiparallel homodimerization of

129   the receptor ectodomain as part of its physiological function (Figures 1G and 1K).[14] Therefore,

130   the receptor surface that contacts the WEEV spike protein is occluded in the PCDH10 homodimer,

131   and only the monomeric form of PCDH10 may bind the WEEV spike protein to facilitate viral entry

132   (Figure S3G).

133

134   **Assessment of WEEV–PCDH10 interactions**

135   The WEEV CBA87 spike protein contacts fifteen residues on human PCDH10 EC1 (Figure

136   S6C). These PCDH10 residues are highly conserved among PCDH10 orthologs that can serve

137   as WEEV receptors,[10] which in addition to human PCDH10 includes the murine, equine, avian,

138   and reptilian PCDH10 orthologs. To evaluate the importance of individual interactions of the

139   WEEV spike protein, we performed infectivity assays on K562 cells, a lymphoblast-derived cell

140   line that does not express PCDH10.[10,31] We transduced K562 cells with a truncated PCDH10

141   construct containing only wild-type or mutated versions of PCDH10 EC1 as a minimal receptor

142   fragment (Figure 1A). For infectivity assays, we chose the 71V1658 (71V) WEEV strain, a North

143   American strain that binds PCDH10 but not VLDLR or ApoER2 (Figure 1B).[10]

144   For most of the WEEV-PCDH10 interface, replacing with alanine individual or multiple

145   PCDH10 EC1 residues that contact the WEEV spike protein had no effect on WEEV 71V RVP

146   entry (Figures 1L and S8). However, individually replacing with alanine two EC1 residues that

147   make polar contacts with the central arch of the E2 β-ribbon connector (N40A or R42A) diminished

148   WEEV 71V RVP infection; simultaneous replacement of both residues with alanine completely

149   abolished entry (Figure 1L). Furthermore, the EC1 P39R substitution, which would introduce steric

150   clashes with nearby residues in the E2 β-ribbon connector, completely abrogated WEEV 71V

151   RVP entry (Figure 1L). Thus, in most cases, the large interaction interface between PCDH10 EC1

152   and the WEEV spike protein is highly tolerant of substitutions that would alter individual contacts

153   with the receptor.

154

155   **Structure of WEEV bound to avian PCDH10**

156   The Imperial 181 (lineage B3) WEEV strain was recovered from a mosquito pool in

157   California in 2005 and is nonpathogenic in animal models.[4,24] Imperial 181 can bind sparrow (*P.*

158   *domesticus*) PCDH10 but not human PCDH10 as a receptor (Figure 1B).[10] We used enzyme-

159   linked immunosorbent assays (ELISAs) with VLPs and human and sparrow $PCDH10_{EC1}$–Fc

160   fusion proteins to compare half maximal effective concentrations (EC_{50}) values as a surrogate for

161   affinity measurements. As expected, sparrow $PCDH10_{EC1}$–Fc, but not human $PCDH10_{EC1}$–Fc,

162   bound to Imperial 181 VLPs (Figures 2A and S2F). While sparrow $PCDH10_{EC1}$–Fc bound

163   McMillan (lineage A) and CBA87 (lineage C) VLPs with comparable apparent affinities (~ 1 nM),

164   human $PCDH10_{EC1}$–Fc bound both VLPs with vastly different apparent affinities (3.8 μM and 77

165   nM, respectively) (Figures 2A and S2F). Interestingly, sparrow $PCDH10_{EC1}$–Fc bound Imperial

166   181 VLPs much less tightly (2.6 μM) than it bound McMillan (1 nM) or CBA87 VLPs (1 nM)

167   (Figures 2A and S2F).

168   To determine why the WEEV Imperial 181 binds sparrow but not human PCDH10, we

169   determined the cryo-EM structure of Imperial 181 VLPs bound to the EC1 repeat of sparrow

170   PCDH10 (Figures 2B, S4B and S7A–D). The global resolution of the map of the receptor-bound

171   (q3) spike was 2.8 Å (masked spike protein trimer) (Table S2). When the human and sparrow

172   PCDH10-bound WEEV structures are compared, the overall binding mode and contact residues

173   are similar (Figures 2C, S7E, and S9A). In the structure of CBA87 bound to human PCDH10, E2

174   L149 is in a cluster of hydrophobic residues that interacts with PCDH10 EC1; the analogous

175   residue in the E2 protein of Imperial 181, Q149, does not contact EC1, with its polar side chain

176   positioned towards a mostly hydrophobic interface (Figures 2D and 2E). On the receptor side of

177   the interface, the side chain of sparrow PCDH10 residue R89 makes multiple polar contacts with

178   Imperial 181 E2 residues T23 and P24 (Figure 2F). However, in human PCDH10, R89 is replaced

179   by a glutamine (Q89) and the side chain of this residue only contacts the backbone carbonyl of

180   WEEV E2 residue P24, thus providing weaker contributions to the interaction with the receptor

181   (Figure 2G). Additionally, the side chain of residue L74 in sparrow PCDH10 is near a hydrophobic

182   pocket that involves E1' fusion loop residue W89 (Figure 2H). L74 in sparrow PCDH10 is replaced

183   by a valine in human PCDH10, with the valine side chain positioned further from the pocket and

184   unable to contact E1' fusion loop residue W89 (Figure 2I).

185

186   **An E2 polymorphism drives PCDH10 ortholog dependencies**

187   The leucine residue at WEEV E2 position 149 is highly conserved among WEEV strains

188   in lineage A, B1, B2, and even some B3 strains, and it is only replaced by a glutamine in Imperial

189   181 and in two additional recent lineage B3 strains that were the most recently isolated in the

190   USA (2005) (Figures 2J, S9A and S10). We had previously tested one of these additional B3

191   strains (R02PV003422B) and found that it also does not bind human PCDH10 (Figure 1B).[10]

192   Given that the L149Q substitution would disrupt key hydrophobic contacts WEEV E2 L149 would

193   otherwise make with PCDH10 EC1, we sought to determine whether the leucine at E2 residue

194   position 149 impairs WEEV's ability to bind human PCDH10. We introduced the E2 L149Q

195   mutation into Fleming (lineage A) RVPs, which can bind human PCDH10, VLDLR, and ApoER2

196   as receptors.[10] We used the mutant Fleming RVPs to conduct infectivity assays in K562 cells

197   overexpressing human PCDH10, with human VLDLR or human MXRA8 included as controls.

198   Fleming RVPs containing the E2 L149Q mutation could not infect cells expressing human

199   PCDH10 but could still recognize human VLDLR (Figure 2K). Thus, the L149Q polymorphism

200   likely explains the inability of some B3 strains to bind human PCDH10.

201

202   **Structural basis for VLDLR recognition**

203   Lineage A WEEV strains, which were isolated in the 1930–1940s in North America, are

204   highly pathogenic in animal models.[24] We previously found that lineage A strains, in addition to

205   binding PCDH10, also bind VLDLR and ApoER2 (Figure 1B).[10] The VLDLR ligand-binding domain

206   (LBD) contains eight LDLR class A (LA) repeats (Figure S12A), which are cysteine-rich domains

207   that contain a Ca^{2+} ion coordinated by multiple acidic residues next to an aromatic residue.[32] The

208   aromatic residue and neighboring acidic residues usually interact with basic residues on

209   physiological ligands and viruses.[16,17,19-22,33-36] Importantly, the critical basic residues on the E2 or

210   E1 proteins of alphaviruses that bind to LA repeats are not conserved among alphaviruses

211   (Figures S6A and S6B).[17,19-22,37] Thus, where LA repeats bind the WEEV spike protein cannot be

212   predicted using previously determined structures.

213   We first sought to map LA repeat dependencies of WEEV lineage A strain McMillan, a

214   strain that was isolated from a human individual in Canada in 1941. We used K562 cells stably

215   expressing VLDLR truncation constructs in which the LBD is replaced by single LA repeats

216   (Figures S12A and S12B). WEEV McMillan could infect cells expressing single LA repeat

217   constructs of LA1, LA2, LA3, and LA5 (Figures 3A and S12C). Interestingly, the LA repeat binding

218   preferences of WEEV McMillan are different than those described for other alphaviruses (EEEV,

219   Semliki Forest virus, and Sindbis virus).[19-21,37]

220   We determined the cryo-EM structure of $VLDLR_{LBD}$–Fc-bound to WEEV McMillan q3

221   spikes at a resolution of 2.9 Å (Figures S4C and S13A–C; Table S2). In the structure of the

222   receptor-bound spike protein, two LA repeats bind clefts and only contact the E2'-E1' protomer

223   (E2'-E1') (Figures 3B–D). Our ability to visualize individual side chains in our high-resolution maps

224   allowed us to unambiguously build LA1 and LA2, with LA1 positioned deepest within the cleft (site

225   1) (Figures 3D and S13D). This binding mode was also consistent with our observation that WEEV

226   RVPs could infect K562 cells expressing VLDLR LA1 or LA2 (Figure 3A).

227   During interactions with VLDLR LA repeats, LA1 and LA2 bury 746 Å^2 of surface area on

228   the McMillan spike (Figure S5A). The LA repeat Ca^{2+}-coordinating acidic residues usually make

229   critical contacts with one or two basic residues (lysines or arginines) on ligands, while the adjacent

230   LA repeat aromatic residue stacks against the aliphatic portion of the lysine or arginine side

231   chain.[33,34] In site 1 of the VLDLR-bound WEEV complex, the side chains of LA1 Ca^{2+}-coordinating

232   acidic residues encircle WEEV E1 residue K227, and the aliphatic portion of K227 stacks against

233   LA1 W50 (Figure 3E). Acidic residues in LA1 also contact two E2 domain B residues, K177 and

234   R224 (Figures 3E and S5F). On the second LA repeat binding site that is more distal from the

235   viral membrane (site 2), the side chains of LA2 Ca^{2+}-coordinating acidic residues interact with

236   K190 on E2' domain B, with the aliphatic portion of the E2 K190 side chain stacking against W89

237   in the LA repeat (Figure 3F). Additional polar contacts that involve the side chain or main chain

238   atoms of WEEV E2 residues K181, Q214 and S178, and LA1 residue D94 and R88, further anchor

239   the LA repeat into place. The WEEV McMillan VLDLR binding mode is distinct from how EEEV,

240   SFV, and VEEV interact with LA repeats,[16,17,20,22] indicating that McMillan independently evolved

241   its solution for binding LA repeats (Figure S14).

242   We tested the importance of WEEV McMillan-VLDLR contact residues using infectivity

243   assays with wild-type or mutant WEEV McMillan RVPs on K562 cells expressing receptors. E1

244   residue K227 (site 1) and E2 residue K190 (site 2) are universally conserved in WEEV strains

245   (Figures S9B, S10 and S11). WEEV McMillan RVPs containing either the E1 K227A (site 1) or

246   E2 K190A (site 2) mutations were unable to infect K562 cells expressing VLDLR, despite retaining

247   the ability to infect cells expressing human PCDH10 (Figure 3G). This observation suggests that

248   simultaneous LA repeat engagement of sites 1 and 2 on the WEEV McMillan spike protein is

249   required for efficient VLDLR binding.

250   All lineage B strains we had previously tested do not bind to VLDLR or ApoER2.[10] We next

251   tested whether polymorphisms on the spike protein in site 1 (R224K) or site 2 (K181E or Q214R)

252   explain why these strains do not bind VLDLR or ApoER2 (Figure S9B). The E2 R224K substitution

253   when introduced into McMillan RVPs did not prevent infectivity of K562 cells expressing VLDLR,

254   suggesting that lysine and arginine are interchangeable at this position (Figure 3G). However, the

255   K181E or Q214R substitutions when individually introduced into WEEV McMillan RVPs abolished

256   infectivity of K562 cells expressing VLDLR (Figure 3G). These data suggest that K181 and Q214

257   are required for VLDLR binding by McMillan. The E2 Q214R substitution, in addition to impairing

258   VLDLR binding, unexpectedly also prevented WEEV McMillan RVP infection of cells expressing

259   PCDH10 (Figure 3G), despite E2 residue 214 not being near the PCDH10 binding site. Because

260   R214 can make a salt bridge with E181, as observed in the CBA87 spike protein structure (Figure

261   S13E), we hypothesized that the E2 R214 substitution destabilizes E2 domain B of the WEEV

262   McMillan spike protein by positioning three basic residues near each other (R214, K181, and

263   K190). Consistent with this notion, WEEV McMillan RVPs containing both the K181E and Q214R

264   E2 substitutions, which would allow R214 to make the salt bridge with E181, had the ability to

265   infect K562 cells expressing PCDH10 (Figure 3G).

266

267   **Fleming uses a distinct VLDLR binding site**

268   The lineage A strain Fleming has a glutamate at E2 position 181 (site 2), which, based on

269   our mutational analysis, impairs McMillan binding to VLDLR (Figures 3G and S9B). Yet, Fleming

270   can still bind VLDLR (Figure 3J).[10] In infectivity studies with Fleming mutant RVPs and K562 cells

271   expressing VLDLR, mutation of either E1 residue K227 (site 1) or E2 residue K190 (site 2) had

272   no impact on VLDLR-dependent entry (Figure 3H). We thus examined the sequence of the

273   Fleming spike protein to identify potential binding sites involving unique, surface exposed lysine

274   residues. We identified one such residue near the threefold axis of the Fleming trimeric spike (E2

275   K81; site 3) that is replaced by glutamate or aspartate in all other strains (Figures 3I and S9B).

276   Interestingly, E2 K81 is adjacent to another basic residue, K82, that could also be recruited to

277   participate in LA repeat binding in Fleming E2 (Figure S10). Introducing the E2 K81E substitution

278   into Fleming RVPs abrogated WEEV Fleming RVP infection of K562 cells expressing VLDLR or

279   ApoER2, while preserving PCDH10-dependent entry (Figure 3J). Therefore, we propose that the

280   key determinant of LA repeat binding for WEEV Fleming is near the threefold axis of the trimer in

281   a third potential LA repeat binding site in WEEV spike proteins.

282

283   **E2 substitutions reinstate WEEV neurotropism**

284   PCDH10 and LDLR-related proteins are expressed on brain cells. Imperial 181 does not

285   bind VLDLR, ApoER2, or PCDH10, and has been shown to replicate poorly in the brain of infected

286   mice,[4,24,38] suggesting an impaired ability to infect neurons and cause encephalitis as compared

287   to virulent WEEV strains.

288   To test the hypothesis that Imperial 181's lack of PCDH10, VLDLR, or ApoER2 binding

289   explains its inability to infect neurons, we generated five mutant Imperial 181 RVPs containing

290   the spike protein substitutions at polymorphic sites that should restore binding to PCDH10,

291   VLDLR and ApoER2, or all three receptors. Mutant 1 (Mut-1) RVPs, which contain the E2 Q149L

292   substitution that should restore the human PCDH10 binding site, were able to infect K562 cells

293   expressing human PCDH10 (Figures 4A–C). Mut-2 RVPs, which contain the E2 E81K substitution

294   that should provide a site 3 LA repeat binding site, could infect K562 cells expressing VLDLR or

295   ApoER2, but not PCDH10. Mut-3 RVPs, which contain the Q149L and the E81K (site 3)

296   substitutions, could infect K562 cells expressing PCDH10, VLDLR, or ApoER2. Mut-4 RVPs,

297   which contain the E181K+R214Q substitutions that would restore a site 2 binding site for LA

298   repeats could infect K562 cells expressing VLDLR and ApoER2. Mut-5 RVPs, containing the

299   Q149L and R214Q+E181K substitutions that would restore PCDH10 binding and a site 2 LA

300   repeat binding site, could infect K562 cells expressing all three receptors.

301   Given the importance of E2 residue L149 in allowing WEEV recognition of human

302   PCDH10, we next assessed the relative efficiency of PCDH10 recognition by mutant Imperial 181

303   RVPs containing the Q149L substitution in E2. We infected K562 cells expressing human or

304   sparrow PCDH10 with Imperial 181 RVPs at different multiplicities of infection (MOI), with RVP

305   titers determined on Vero E6 cells. We chose Vero E6 cells to measure RVP titers because we

306   previously found that WEEV Imperial 181 RVPs can infect these cells without binding to PCDH10

307   or LDLR-related proteins.[10]

308   Imperial 181 RVPs were unable to recognize human PCDH10 to infect K562 cells even at

309   an MOI of 4, but recognized sparrow PCDH10 (Figure 4D). However, Imperial 181 RVPs required

310   a much higher MOI than did McMillan and 71V RVPs to reach 50% infection of cells expressing

311   sparrow PCDH10, suggesting that Imperial 181 uses sparrow PCDH10 less efficiently as a

312   receptor. The results of these infectivity assays are consistent with a lower apparent affinity of

313   Imperial 181 VLPs for sparrow PCDH10$_{EC1}$–Fc as compared to McMillan VLPs in ELISA

314   experiments (Figure 2A). Interestingly, we found that Imperial 181 mutant RVPs that contain the

315   Q149L substitution, Mut-1 and Mut-5, not only gained the ability to infect cells expressing human

316   PCDH10, but also were able to more efficiently infect cells expressing sparrow PCDH10 (Figure

317   4D). These observations suggest that the L149Q polymorphism decreases affinity for human and

318   sparrow PCDH10, which is likely explained by the removal of key hydrophobic contacts E2

319   residue L149 makes with PCDH10 EC1 (Figures 2D and 2E). Interestingly, all tested RVPs could

320   infect K562 cells expressing sparrow MXRA8 with similar efficiencies (Figure 4D). This suggests

321   that the E2 L149Q polymorphism does not affect binding to sparrow MXRA8.

322   We next used the five mutant RVPs to infect primary cortical neurons isolated from

323   embryonic mice. Wild-type Imperial 181 RVPs did not infect murine primary neurons (Figures 4E,

324   4F, and S12D). However, RVP mutants 1 through 5, consistent with their ability to bind either

325   PCDH10 or VLDLR/ApoER2, all gained the ability to infect murine primary neurons (Figures 4E,

326   4F, and S12D). Confirming that the infection we observed was specific to the mutant RVPs' newly

327 acquired ability to bind specific receptors, treatment with PCDH10$_{EC1}$–Fc blocked infection by all

328 mutants that should have gained the ability to bind mammalian PCDH10 because they contain

329 the Q149L substitution (Mut-1, Mut-3, and Mut-5) (Figures 4E and 4F). Treatment with the near-

330 universal LDLR family member ligand antagonist receptor-associated protein (RAP), which blocks

331 alphavirus spike protein binding to VLDLR and ApoER2,[39] blocked the entry of Imperial 181

332 mutants that should only bind VLDLR or ApoER2 (Mut-2 and Mut-4) (Figures 4E and 4F). The

333 "Fleming-like" composite Mut-3 was likewise blocked by RAP (Figures 4E and 4F), suggesting

334 that despite containing leucine at E2 position 149 which allows for PCDH10 binding, Mut-3 still

335 critically depends on LDLR-family receptors to infect these neurons. However, the "McMillan-like"

336 composite Mut-5 was not affected by the addition of RAP (Figures 4E and 4F), suggesting that

337 Mut-5, unlike Mut-3, primarily depends on PCDH10 to infect these neurons.

338

339 **Spike protein sequence-based prediction of receptor binding patterns**

340 We hypothesized that knowledge of the E2 polymorphisms that drive the ability of WEEV

341 strains to bind human PCDH10 or VLDLR/ApoER2 would allow us to predict the receptor-binding

342 properties of strains we had not yet evaluated. The sequences of nine WEEV strains isolated in

343 the 2023–2024 outbreak in South America have been made publicly available (Table S1).[7]

344 Phylogenetic analysis places all these strains into a newly designated C lineage (as reported by

345 Campos et al.[7]) that also includes strain CBA87 (Figures 1B and S1). The CBA87 strain was

346 previously isolated from the brain of an infected horse in Argentina in 1958 and is the source

347 strain for the VLPs we used for structural analysis with human PCDH10 EC1.

348 We included in our analysis three South American WEEV strains that have no lineage

349 assignment (AG80-646, isolated in 1980, Ar Enc MV, isolated in 1933, and TR25717, isolated in

350 Guayana in 1959) (Figure 1B). We also included two re-emerging South American strains,

351 EQ1090 (identified in Brazil in 2023) and DILAVE218 (identified in Uruguay in 2023) (lineage C).

352 All these strains contain a leucine at E2 position 149, which we predict would allow them to bind

353   human and sparrow PCDH10 (Figure 2J). We did not expect these strains to bind VLDLR or

354   ApoER2, as they all lack the lysine residues at E2 positions 181 (site 2) or 81 (site 3) required for

355   VLDLR/ApoER2 binding (Figure S9B). Infectivity assays on K562 cells indeed revealed that RVPs

356   for AG80-646, Ar Enc MV, TR25717, and the two re-emerged lineage C strains could bind

357   PCDH10 but not VLDLR or ApoER2 for cellular entry (Figure 5A). In a second experiment, we

358   transduced K562 cells to express orthologs for nonhuman mammal, avian, and reptilian orthologs

359   that WEEV is known to bind in addition to human orthologs of PCDH10 (Figure 5B). AG80-646

360   and two lineage C strains we evaluated, CBA87 (1958) and EQ1090 (2023), bound all tested

361   orthologs (Figure 5B).

362   When we examined polymorphisms in VLDLR binding sites across North American WEEV

363   strains, we found that two lineage B strains we had not previously tested, BFS09997 (sublineage

364   B1, isolated in 1978 from mosquitoes in California, USA) and EP6 (sublineage B2, isolated in

365   1950 from mosquitoes in Missouri, USA), contain a lysine at E2 position 181 (LA repeat binding

366   site 2) (Figure S9B), which may allow these strains to bind VLDLR and ApoER2. Unlike all other

367   lineage B strains we had previously tested, BFS09997 and EP6 RVPs could infect K562 cells that

368   express VLDLR and ApoER2 (Figure 5C). Interestingly, both strains have R214 (Figure S9B),

369   which our mutagenesis studies suggested prevents VLDLR/ApoER2 binding in the context of the

370   McMillan spike protein (Figure 3G). Thus, these two lineage B strains can tolerate the combination

371   of E2 K181 and R214, which could be related to compensatory changes elsewhere in their spike

372   proteins. Thus, our data suggest that E2 K181 is a determinant of VLDLR and ApoER2 binding

373   that can be acquired by strains outside of the ancestral A lineage.

374

375   **Shift in receptors of a South American WEEV strain**

376   AG80-646 is an enzootic WEEV strain that was isolated from mosquitoes in Argentina in

377   1980,[40] and likely represents a lineage that is highly divergent from lineage C (Figures 1B and

378   S1). While all WEEV strains we and others have examined to date can bind avian orthologs of

379 MXRA8,[10,41] unexpectedly, we found that AG80-646 RVPs could not recognize sparrow MXRA8

380 to infect K562 cells, despite the ability to recognize human, murine, equine, sparrow, and reptilian

381 PCDH10 (Figure 5B). Infectivity studies with AG80-646 RVPs at a range of MOIs on K562 cells

382 expressing sparrow MXRA8 suggests that this strain does not have any affinity for sparrow

383 MXRA8 (Figure 5D). This observation suggests that like WEEV lineages in North America, South

384 American WEEV lineages may have also undergone shifts in their receptor-binding properties as

385 they diverged.

386

387 **A WEEV-related alphavirus binds PCDH10**

388 Highlands J virus (HJV) is a North American alphavirus closely related to WEEV that was

389 first isolated in 1960 from a blue jay (*Cyanocitta cristata*) in Florida, USA (Figures 5E and S1;

390 Table S1). HJV is thought to circulate on the East Coast of the USA,[2] with birds as a primary

391 reservoir, and was most recently detected in a red-tail hawk (*Buteo jamaicensis*) in Georgia in

392 2001[42] and in a sandhill crane in *Missisipi* (*Grus canadensis pulla*) in 2012.[43] The virus is

393 pathogenic in certain avian species.[44,45] Although cases of human HJV infections have been

394 documented incidentally in individuals co-infected with St. Louis encephalitis virus,[46] and HJV was

395 associated with a case of fatal equine encephalitis,[47] HJV is not generally considered to be an

396 equine or human pathogen. HJV has no known receptors.

397 Conservation of PCDH10 contact residues in the HJV E2–E1 spike protein sequence,

398 including leucine at a position equivalent to WEEV E2 residue 149, led us to suspect that PCDH10

399 may serve as a receptor for HJV (Figure S9A). Indeed, we found that HJV RVPs could infect cells

400 expressing human, murine, avian, and reptilian orthologs of PCDH10 (Figures 5F–H). Consistent

401 with the lack of the required lysine residues in positions equivalent with WEEV E2 LA repeat

402 binding sites 2 (e.g., K181) or 3 (e.g., K81), HJV could not use VLDLR or ApoER2 to infect cells

403 (Figures 5F and S9B). Interestingly, we also found that avian MXRA8 could serve as a receptor

404   for HJV, consistent with a close evolutionary relationship between HJV with WEEV (Figures 5E

405   and 5G).

406   Unexpectedly, the HJV strain we tested (585-01, isolated in 2001) could not efficiently

407   enter cells expressing equine PCDH10 (Figure 5H). Examination of sequence alignments and the

408   structures revealed that a K177A polymorphism (with respect to WEEV E2 sequence) found in

409   HJV would remove a key salt bridge with PCDH10 (Figures 1H and S9A). The A177K E2

410   substitution, when introduced into the HJV RVPs, allowed these RVPs to more readily infect K562

411   cells expressing equine PCDH10 (Figure 5H). Thus, HJV is another North American alphavirus

412   that can bind PCDH10 orthologs as cellular receptors.

413

414   **Discussion**

415   We report here structures of WEEV bound to two of its structurally unrelated alternate

416   receptors, PCDH10 and VLDLR. The structures allow us to define the polymorphisms in the

417   WEEV E2 spike protein that drive shifts in the receptor-binding properties of strains isolated over

418   the past century.

419   We constructed a phylogenetic tree using the structural polyprotein coding sequences of

420   57 WEEV strains (Figure S1). The phylogenetic tree shows that E2 Q149, which abolishes human

421   PCDH10 binding, is a signature substitution of the most recently isolated North American B3 clade,

422   to which Imperial 181 belongs (Figure S1). Our tree also shows that newer isolates of North

423   American WEEV strains tend to be placed in new clades instead of extending older clades,

424   confirming previous findings of rapid clade displacement in circulating WEEV.[4,48] If clade

425   displacement has continued in the past two decades, the E2 Q149 clade may have displaced

426   older clades and expanded in the continent, marking the epizootic decline of WEEV in North

427   America as function of the inability of these newer WEEV strains to bind human and equine

428   orthologs of PCDH10. Indeed, strains in this clade were isolated in California and Texas (Table

429   S1), suggestive of its geographic expansion. Further environmental sampling is required to test

430   this hypothesis.

431   Strains McMillan and California appear to form a distinct clade within lineage A; this clade

432   can be defined as containing a lysine at E2 position 181. We found that K181 is a contact residue

433   for LA repeats and is a critical determinant of VLDLR and ApoER2 binding (Figures 3F and 3G).

434   This lysine, however, is likely replaced by a glutamate in the common ancestor of WEEV lineage

435   A, given that Fleming contains a glutamate at that position and lies basal to California and

436   McMillan in the phylogenetic tree (Figure S1). Therefore, the clade containing California and

437   McMillan likely evolved from an ancestral strain containing a glutamate at E2 position 181 that

438   acquired a lysine substitution; this ancestral strain went on to spill over and gave rise to large

439   epidemics that spanned over at least a decade in the 1930s–1940s. The McMillan/California clade

440   would later become extinct and displaced. Our identification of two lineage B strains that contain

441   the E2 E181K polymorphism and can bind VLDLR and ApoER2 in addition to PCDH10

442   (BFS09997 and EP6) (Figure 5C) supports the notion that this polymorphism may be a transitory

443   mutation that could arise stochastically. Of note, while the lineage A strains McMillan and

444   California were more extensively passaged, BFS09997 and EP6 were minimally passaged (Table

445   S1), suggesting that E2 K181 is a naturally occurring substitution as opposed to the result of

446   passaging.

447   Our mutational analysis suggests that the Fleming strain uses a different surface to bind

448   VLDLR and ApoER2. This strain likely represents a separate lineage A clade that circulated at

449   the same time as strains California and McMillan. As an alternative explanation, a previous study

450   proposed that the E2 K81 polymorphism in Fleming may be a result of cell culture adaptation

451   during passaging.[49] Strain Mn548, a group B2 strain also containing E2 K81 (Figures S1 and

452   S9B), has unknown source of isolation and passage history, making it difficult to assess the origin

453   of the E2 K81 polymorphism. Nonetheless, our finding that the E81K polymorphism allows WEEV

454   strains to bind VLDLR and ApoER2 to infect neurons suggest that this additional potential site of

455   LA repeat binding would be important to monitor during environmental viral sampling efforts.

456   Strains from the South American C lineage, which is responsible for the recent re-

457   emergence of WEEV in South America,[7] all contain a leucine at E2 position 149. The leucine at

458   this position should allow isolated strains to bind human and equine PCDH10 in addition to avian

459   PCDH10. While WEEV has submerged as a human pathogen in North America, in contrast, in

460   South America, serological evidence suggests that WEEV continued to spill over into epizootic

461   hosts well into the 21st century.[50-52] The ability of WEEV to persist in epizootic circulation in South

462   America may explain the preservation of E2 L149, as well as mammalian PCDH10 recognition,

463   by lineage C in South America.

464   Our structural analysis of PCDH10- or VLDLR-bound WEEV reveals an overlapping

465   binding site for multiple structurally unrelated receptors. It also explains how receptor-decoy

466   proteins comprising the EC1 domain of PCDH10 or the VLDLR LBD can block access to PCDH10,

467   VLDLR, and ApoER2, and protect mice from lethal challenge by the highly virulent lineage A strain

468   McMillan[10,23]. Additionally, receptor decoy proteins that contain VLDLR LA1-LA2, which are

469   known to be protective against EEEV challenge in mice,[20] would presumably also protect against

470   WEEV strains that bind LDLR-related proteins.

471   Interestingly, the EC1 residues of PCDH10 that interact with WEEV are not conserved in

472   its two closest δ2 protocadherin family members, PCDH17 and PCDH19, suggesting that WEEV

473   cannot infect cells by binding to PCDH17 or PCDH19 (Figure S6D).[14] Although we used a

474   construct that contains only EC1 for structural analysis, the PCDH10 ectodomain includes six

475   cadherin repeats and is thought to be relatively rigid, as calcium ions are coordinated by adjacent

476   repeats. Superimposing the X-ray crystal structure of the PCDH10 ectodomain containing EC

477   repeats 1 through 6[14] with our structure of WEEV bound to PCDH10 EC1 revealed steric clash at

478   the EC2 domain if all three clefts of the trimeric WEEV spike are bound by the receptor (Figure

479   S3H). We thus suspect that each WEEV trimeric spike may engage only one PCDH10 molecule.

480   The WEEV PCDH10 binding mode may thus parallel how rhinovirus-C interacts with cadherin-

481   related protein 3 (CDHR3).[53] In the CDHR3–rhinovirus-C interaction, the most membrane distal

482   repeat of CDHR3 (EC1) also interacts with the virus but the subsequent repeat (EC2) limits

483   occupancy through steric hindrance.[53]

484   A previous study by Mossel et al. examining the effects of WEEV E2 polymorphism on

485   pathogenicity in mice showed that introducing the E2 Q214R mutation, which our assays revealed

486   would prevent McMillan from binding PCDH10, VLDLR, or ApoER2 (Figure 3G), decreases

487   McMillan's mortality in mice (from 100% with the wild-type virus down to 10% with the Q214R

488   McMillan mutant) (Figure S9C). Introducing the K181E mutation in WEEV McMillan, which our

489   assays revealed would impair binding to VLDLR and ApoER2 but would still allow for PCDH10

490   binding (Figure 3G), had a milder effect in decreasing mortality in mice to 70%, while delaying the

491   mean time to death by two days (Figure S9C).[38] Thus, the ability to bind PCDH10, VLDLR, and

492   ApoER2 likely influences WEEV pathogenicity in mice. The structural information provided in our

493   study will facilitate additional studies that directly evaluate the individual contribution of WEEV

494   mammalian receptors to neurovirulence in animal models.

495   Our findings provide a guide for estimating the potential threat any given WEEV strain

496   might pose based on sequence polymorphisms in its viral spike protein as determinants of virus

497   receptor dependencies and propensities for neurotropism. They should thus facilitate

498   environmental surveillance and bolster future outbreak preparedness.

499

500

Figure 1. Structural basis for WEEV recognition of human PCDH10. (A) Schematic diagrams of PCDH10 and Flag-tagged constructs. (B) Partial phylogenetic tree and summary of infectivity assays with GFP-expressing RVPs for various WEEV strains and Highlands J virus in K562 cells stably expressing the indicated receptors. Strains newly tested in this study are indicated with black triangles. Other results were previously reported in Li et al.[10] (C) Cryo-EM maps of human PCDH10$_{EC1}$–Fc bound to WEEV CBA87 VLP. WEEV E2 and E1 and PCDH10 EC1 are shown in purple, green, and pink, respectively. The 5-fold (i5), 3-fold (i3), and 2-fold (i2) icosahedral symmetry axes are indicated with a closed circle, triangle, and hexagon, respectively. The icosahedral threefold (i3) and quasi-three-fold (q3) spikes are circled and indicated. (D) Ribbon diagram of a single WEEV E2–E1 protomer and PCDH10 EC1 repeat fitted into its associated cryo-EM density map. The angle with which EC1 is inserted into the cleft relative to the threefold axis of spike protein trimer is indicated. E2 and E1 domains are indicated. Dashed lines indicate the position of the viral membrane. TM: transmembrane. (E) Surface representation of the

PCDH10 EC1-bound WEEV CBA87 spike protein. One of the three PCDH10 EC1 molecules is shown in ribbon representation. Clusters of spike protein residues that interact with EC1 are shown in yellow. Details for the indicated interacting regions are shown in panels F to J. (F–J) PCDH10 EC1 interactions with the WEEV E2–E1 protomer (F and G) and E2'–E1' protomer (H-J). WEEV E2 L149, a key polymorphic residue, is indicated with an asterisk. Hydrogen bonds and salt bridges are shown as dashed lines. (K) Interaction interface of human PCDH10 EC1 and EC4 in a crystal structure of the PCDH10 EC1–EC4 homodimer (PDB: 6VFW).[14] (L) Infection of K562 cells stably expressing wild-type and mutant human PCDH10 EC1 constructs by GFP-expressing WEEV RVP (strain 71V1658). Infection was quantified by flow cytometry. See Figure S8 for flow cytometry gating strategy and cell surface receptor staining. Data are mean ± s.d. from three experiments performed in duplicates or triplicates (n=3) (L). One-way ANOVA with Dunnett's multiple comparisons test, ****P<0.0001 compared to stalk-Flag (L).
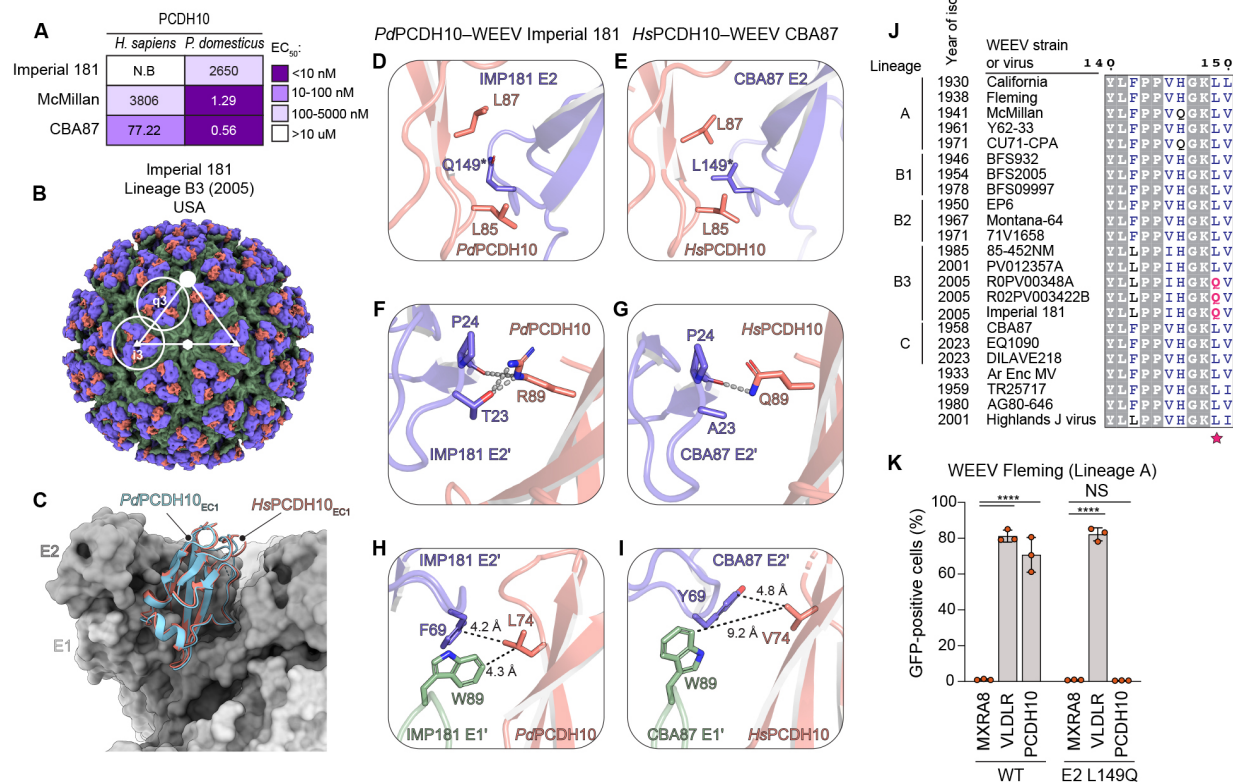
Figure 2. WEEV recognition of avian PCDH10. (A) Summary of the EC_{50} values measured in ELISAs with human (*Hs*) $PCDH10_{EC1}$–Fc or *P. domesticus* (*Pd*) $PCDH10_{EC1}$–Fc on immobilized WEEV VLPs for the indicated strains. See Figure S2F for additional information. (B) Cryo-EM map of *Pd*$PCDH10_{EC1}$–Fc bound to WEEV Imperial 181 VLP. E2, E1, and PCDH10 are colored purple, green, and pink, respectively. (C) Superposition of the cryo-EM structure of *Pd*PCDH10 EC1 (cyan) bound to the WEEV Imperial 181 spike protein and *Hs*PCDH10 EC1 (pink) bound to the CBA87 spike protein. PCDH10 EC1 is shown as a ribbon diagram and the spike protein subunits are shown in dark (E2) and light (E1) gray. (D–I) Side-by-side comparison of the contact residues of *Pd*PCDH10-bound Imperial 181 (D, F, H) and *Hs*PCDH10-bound CBA87 (E, G, I). Residues that participate in interactions are indicated, with polar contacts shown as gray dashed lines. Dashed lines shown in black indicate the closest distances between PCDH10 residue L74 and atoms on the WEEV spike protein for the protomers shown (H, I). The residue at E2 position 149, a key polymorphic residue in the PCDH10 interface, is highlighted with an asterisk. IMP181: Imperial 181. (J) Partial sequence alignment of WEEV E2 proteins, generated using ESPript3.[54] The key polymorphic residue at position 149 is indicated with a star. Light gray background indicates residues that are completely conserved. Boxed residues indicate positions where a single majority residue or multiple chemically similar residues are present. These residues are shown in dark blue. Glutamine at E2 position 149 (indicated with a star) is colored pink. See also Figures S9A and S10 for additional information. (K) K562 cells stably expressing human MXRA8, VLDLR or PCDH10 were infected with GFP-expressing wild-type or L149Q mutant Fleming RVPs. Infection was quantified by flow cytometry. Data are mean ± s.d. from two experiments performed in duplicates or triplicates (n=3) (K). Two-way ANOVA with Dunnett's multiple comparisons test, ****P<0.0001 (K).
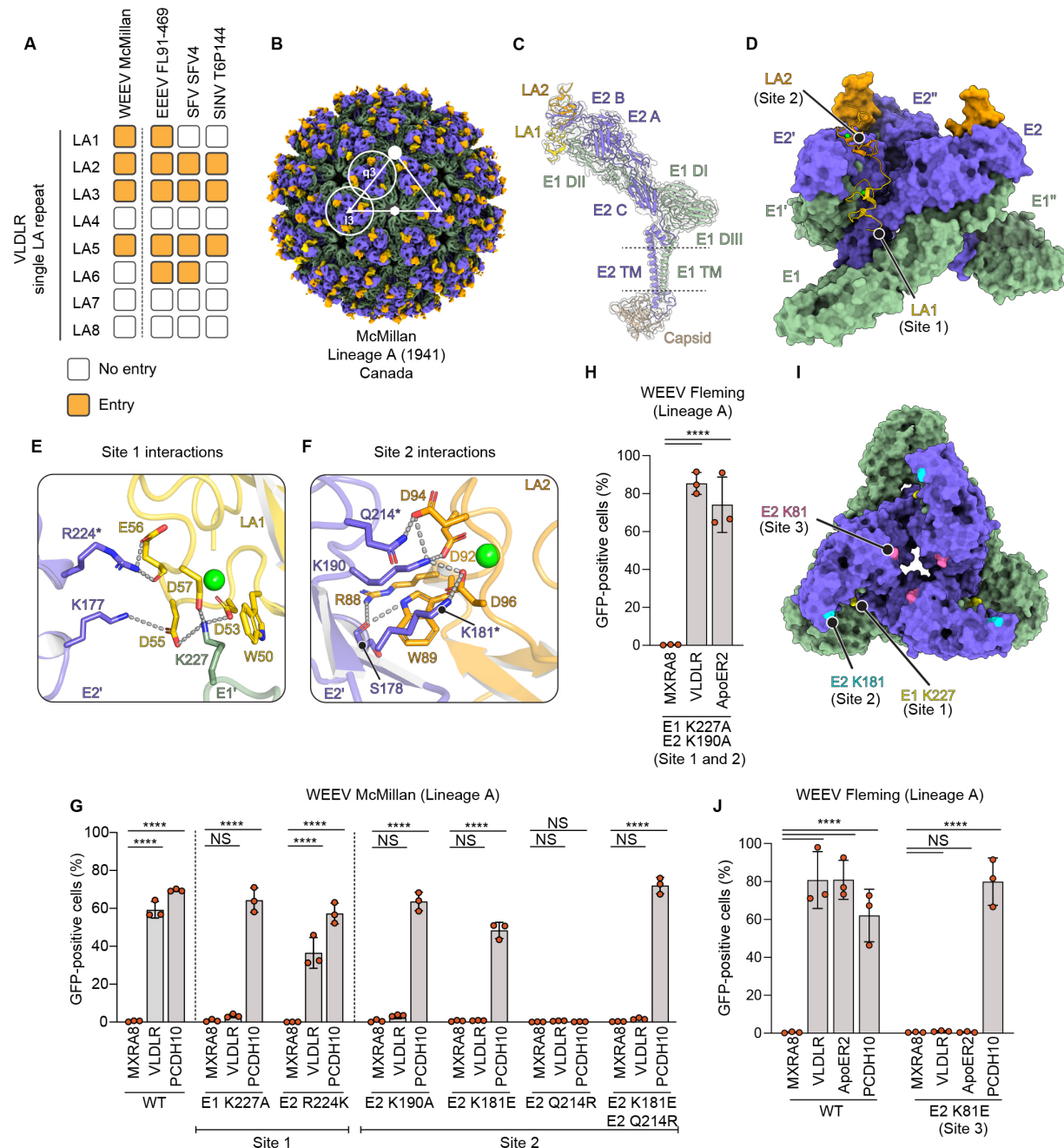
Figure 3. VLDLR recognition by ancestral WEEV strains. (A) Summary of the results of infectivity studies with GFP-expressing RVPs for the indicated alphaviruses with K562 cells expressing VLDLR single LA repeat constructs, with entry quantified using flow cytometry. Infectivity with WEEV McMillan is reported here (see Figures S9A–C) and results for EEEV, SFV, and SINV were previously reported.[19] "Entry" indicates that the construct mediates statistically significant (p < 0.05) RVP infection when compared to a control construct that lacks a ligand-binding domain (LBD). (B) Cryo-EM map VLDLR$_{LBD}$–Fc bound to WEEV McMillan VLP. E2, E1, and VLDLR LA1 and LA2 are colored in purple, green, light yellow, and dark yellow, respectively. The 5-fold (i5), 3-fold (i3), and 2-fold (i2) icosahedral symmetry axes are indicated respectively with solid circle, triangle, and hexagon. The icosahedral threefold spike (i3) and quasi-threefold spike (q3) are circled and labeled. (C) Ribbon diagram of a single WEEV E2–E1 protomer and LA1–2 from the VLDLR LBD fitted into the cryo-EM density map. E2 and E1 domains are indicated.

565 Dashed lines indicate the position of the viral membrane. TM: transmembrane. (D) Surface
566 representation of the VLDLR-bound WEEV CBA87 spike protein. One of the three VLDLR LA1–
567 2 segments are shown in ribbon representation. (E and F) Contacts between WEEV McMillan and
568 VLDLR LA1 (E) or LA2 (F). Polar contacts are shown as dashed lines. Ca^{2+} ions are shown as
569 green spheres. Polymorphic residues that contact VLDLR are highlighted with asterisks. (G) K562
570 cells expressing human MXRA8, VLDLR, or PCDH10 were infected by GFP-expressing wild-type
571 or mutant WEEV McMillan RVPs. (H) K562 cells stably expressing human MXRA8, VLDLR, or
572 ApoER2 were infected with GFP-expressing wild-type or E1 K227A (site 1) + E2 K190A (site 2)
573 mutant WEEV Fleming RVPs. Infection was quantified by flow cytometry. (I) Top view of the
574 WEEV trimeric spike showing three potential binding sites on WEEV E2 and E1 for VLDLR LA
575 repeats. K181 (site 1, cyan) on the E2 glycoprotein and K227 (site 2, yellow) on the E1
576 glycoprotein are critical contact residues with VLDLR in WEEV McMillan. A lysine at position 81
577 (site 3, pink) in WEEV Fleming E2 likely binds VLDLR LA repeats. (J) K562 cells stably expressing
578 human MXRA8, VLDLR, or ApoER2 were infected with GFP-expressing wild-type or E2 K81E
579 (site 3) mutant WEEV Fleming RVPs. Infection was quantified by flow cytometry. Data are mean
580 ± s.d. from three experiments performed in triplicates (n=3) (G, H, J). Two-way ANOVA with
581 Dunnett's multiple comparisons test, ****P<0.0001 (G, H, I).

582
583

584
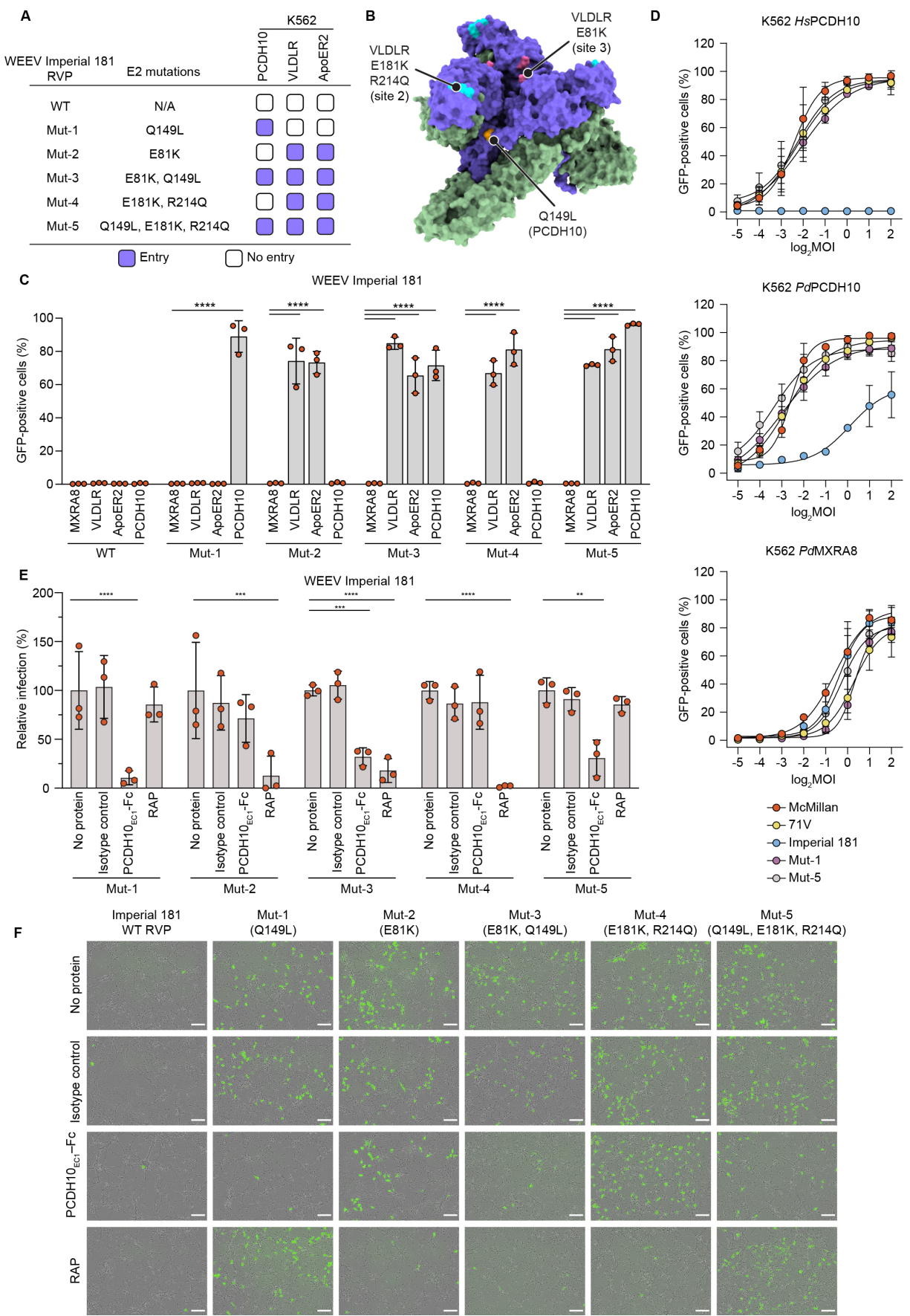
Figure 4. WEEV E2 protein polymorphisms that alter receptor recognition determine WEEV neurotropism. (A) List of mutations generated for WEEV Imperial 181 and summary of K562 infectivity assay as performed in (C). (B) Side view of the WEEV spike highlighting mutated residues on the E2 glycoprotein. (C) K562 cells expressing MXRA8, VLDLR, ApoER2, or PCDH10 were infected with wild-type or mutant Imperial 181 RVPs. Infection was monitored by flow cytometry. (D) K562 cells expressing human PCDH10 (HsPCDH10), sparrow PCDH10 (PdMXRA8), or sparrow MXRA8 (PdMXRA8) were infected with the indicated GFP-expressing RVPs at various MOIs, as pre-determined of Vero E6 cells (see Methods for additional information). Infection was quantified by flow cytometry. (E) Primary murine cortical neurons were infected with GFP-expressing wild-type or mutant WEEV Imperial 181 RVPs in the presence of 316 µg ml^{-1} PCDH10$_{EC1}$–Fc, 100 µg ml^{-1} RAP, or an isotype control. Infection was monitored through a live cell imaging system. (F) Representative merged images of GFP and bright field are shown for the experiment in (E). Scale bars are 100 µm. Data are mean ± s.d. from three experiments performed in duplicates or triplicates (n=3) (C, D, E). One-way ANOVA with Dunnett's multiple comparisons test, ****P<0.0001 (C, D). Two-way ANOVA with Šídák's multiple comparisons test, ****P<0.0001 (E).

602

Figure 5. Prediction of alphavirus receptor usage based on spike protein sequences. (A) K562 cells expressing human MXRA8, VLDLR, ApoER2, or PCDH10 were infected with GFP-expressing RVPs for the indicated South American WEEV strains. (B) K562 cells expressing the indicated orthologs of PCDH10 or MXRA8 were infected with GFP-expressing RVPs for the indicated South American WEEV strains. (C) K562 cells expressing human MXRA8, VLDLR, ApoER2, or PCDH10 were infected with GFP-expressing WEEV BFS09997 (lineage B1) and WEEV EP6 (lineage B2) RVPs. (D) K562 cells expressing human PCDH10 (*Hs*PCDH10), sparrow PCDH10 (*Pd*MXRA8), or sparrow MXRA8 (*Pd*MXRA8) were infected with GFP-expressing WEEV AG80-646 RVPs at the indicated MOIs, as determined on Vero E6 cells (see Methods for

613   additional information). (E) Maximum likelihood phylogenetic tree of select alphaviruses (WEEV,
614   highlands J virus (HJV), Sindbis virus (SINV), VEEV, Madariaga virus (MADV), EEEV,
615   Chikungunya virus (CHIKV), O'nyong'nyong virus (ONNV), Mayaro virus (MAYV), Semliki Forest
616   virus (SFV), Ross River virus (RRV), Getah virus (GETV)) using the coding sequences of the
617   structural polyprotein genes. See Table S1 for strain information. (F) K562 cells expressing
618   human MXRA8, VLDLR, ApoER2, or PCDH10 were infected with GFP-expressing HJV RVPs.
619   (G) K562 cells expressing *Hs*PCDH10, *Pd*PCDH10, *Hs*MXRA8, or *Pd*MXRA8 were infected with
620   GFP-expressing HJV RVPs. (H) K562 cells expressing PCDH10 orthologs were infected with
621   GFP-expressing wild-type (WT) and HJV E2 A177K mutant RVPs. This experiment was
622   performed with an MOI of 1 for WT and mutant RVPs measured on Vero E6 cells. Infection was
623   quantified by flow cytometry. Data are mean ± s.d. from three experiments performed in duplicates
624   or triplicates (n=3) (A, B, C, D, F, G, and H). Two-way ANOVA with Dunnett's multiple
625   comparisons test (A, B, C). Two-way ANOVA with Šídák's multiple comparisons test (H). One-
626   way ANOVA with Dunnett's multiple comparisons test (F, G)
627
628
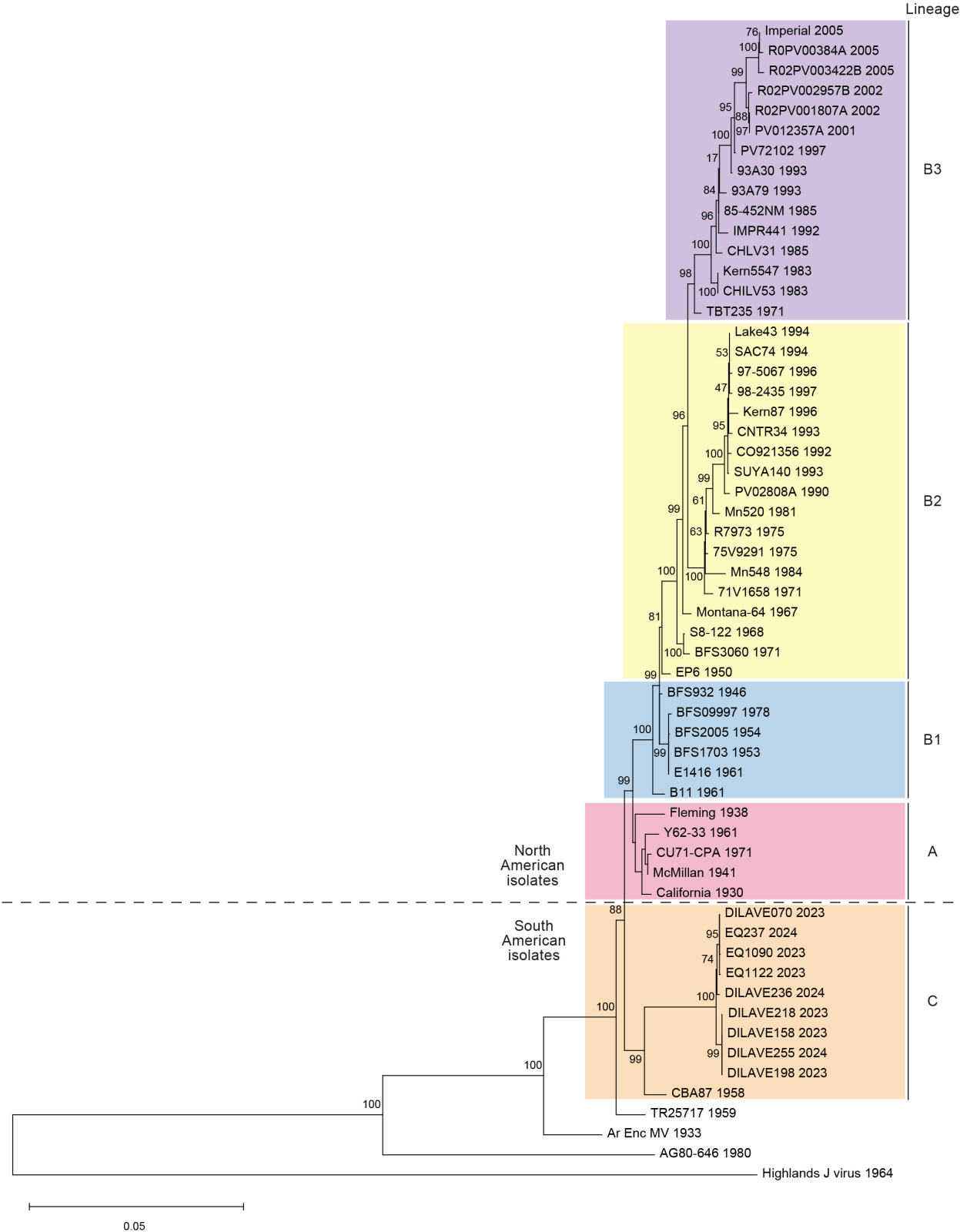
Supplementary Figure 1. Phylogenetic tree of WEEV strains and Highlands J virus. Maximum likelihood phylogenetic tree of 57 WEEV strains using the coding sequences of the structural polyprotein genes. Highlands J virus strain 64A-1519 (GenBank: KT429021) is also included. Scale bar represents 0.05 nucleotide substitutions per site. SFV strain SFV4, VEEV

634   strain TC-83, and MADV strain 267113 were included in the phylogenetic analysis (not shown).
635   Numbers at nodes indicate bootstrap values. In cases in which the branches are too small,
636   bootstrap values may not be shown. The three lineages (A, B, and C) and B sublineages (B1, B2,
637   and B3) are indicated. Taxon labels include strain name and year of isolation. GenBank accession
638   numbers are provided in Table S1.
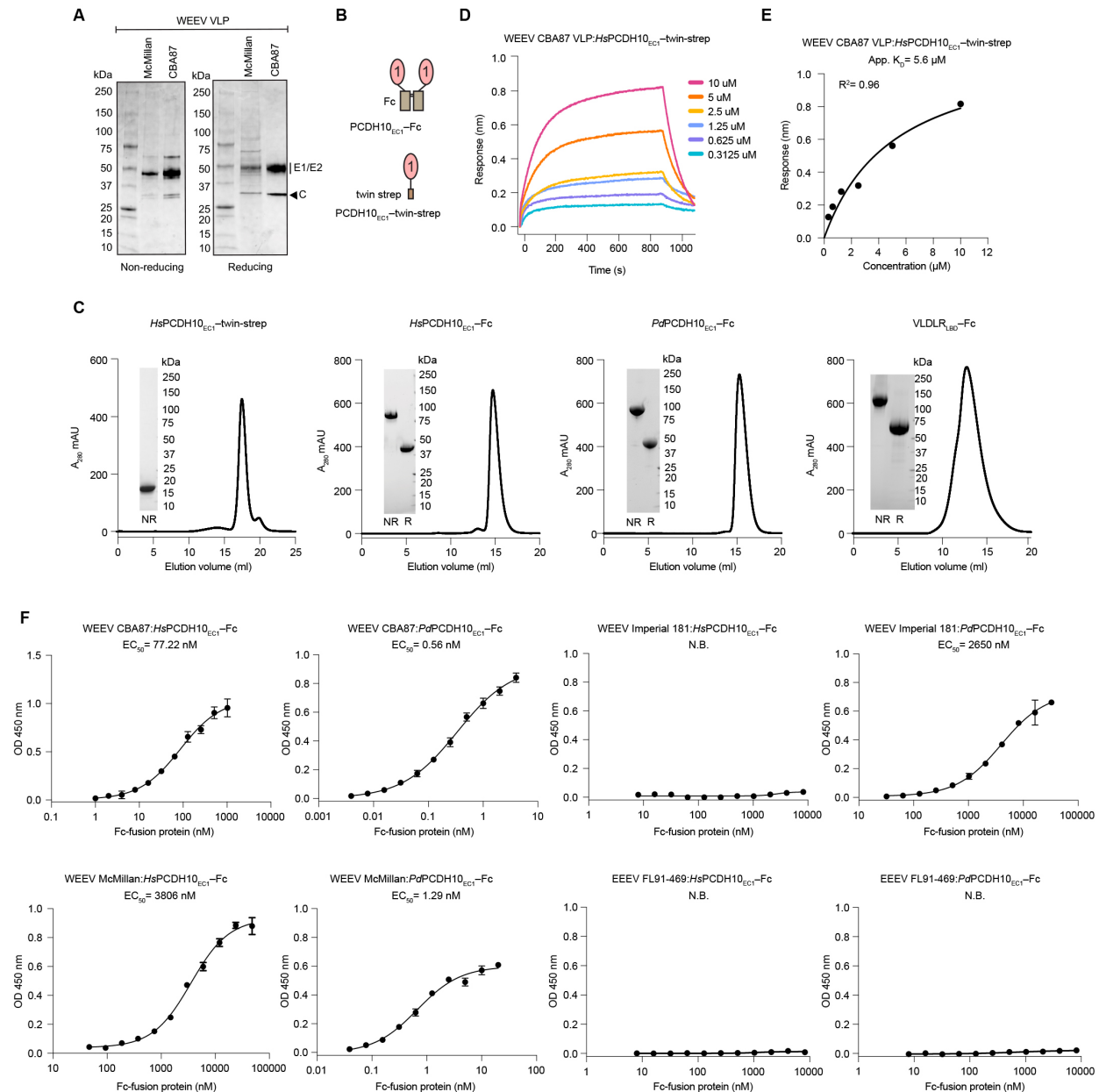
Supplementary Figure 2. Binding experiments with PCDH10 EC1 and WEEV VLPs.
(A) Coomassie-stained SDS-PAGE gel of purified VLPs. The experiment was performed twice, and representative gel images are shown. (B) Schematic diagrams of the $PCDH10_{EC1}$–Fc and the $PCDH10_{EC1}$ twin-strep tag constructs. (C) Size exclusion chromatography of Fc-fusion and twin-strep tagged proteins. Insets are SDS-PAGE gels of pooled peak fractions, which were visualized using a stain-free imaging system.(D) Biolayer interferometry binding analysis of $HsPCDH10_{EC1}$–twin-strep with immobilized WEEV CBA87 VLPs. (E) Scatchard plot for the binding data of $HsPCDH10_{EC1}$–twin-strep with WEEV CBA87 VLPs shown in (D). The measured apparent affinity is indicated. (F) Representative ELISA results showing the binding of the $HsPCDH10_{EC1}$–Fc or $PdPCDH10_{EC1}$–Fc to WEEV CBA87, WEEV McMillan, WEEV Imperial 181, or EEEV FL91-469 VLPs. The experiment was performed three times and representative data are shown. EC_{50} values shown are the mean of three independent experiments.
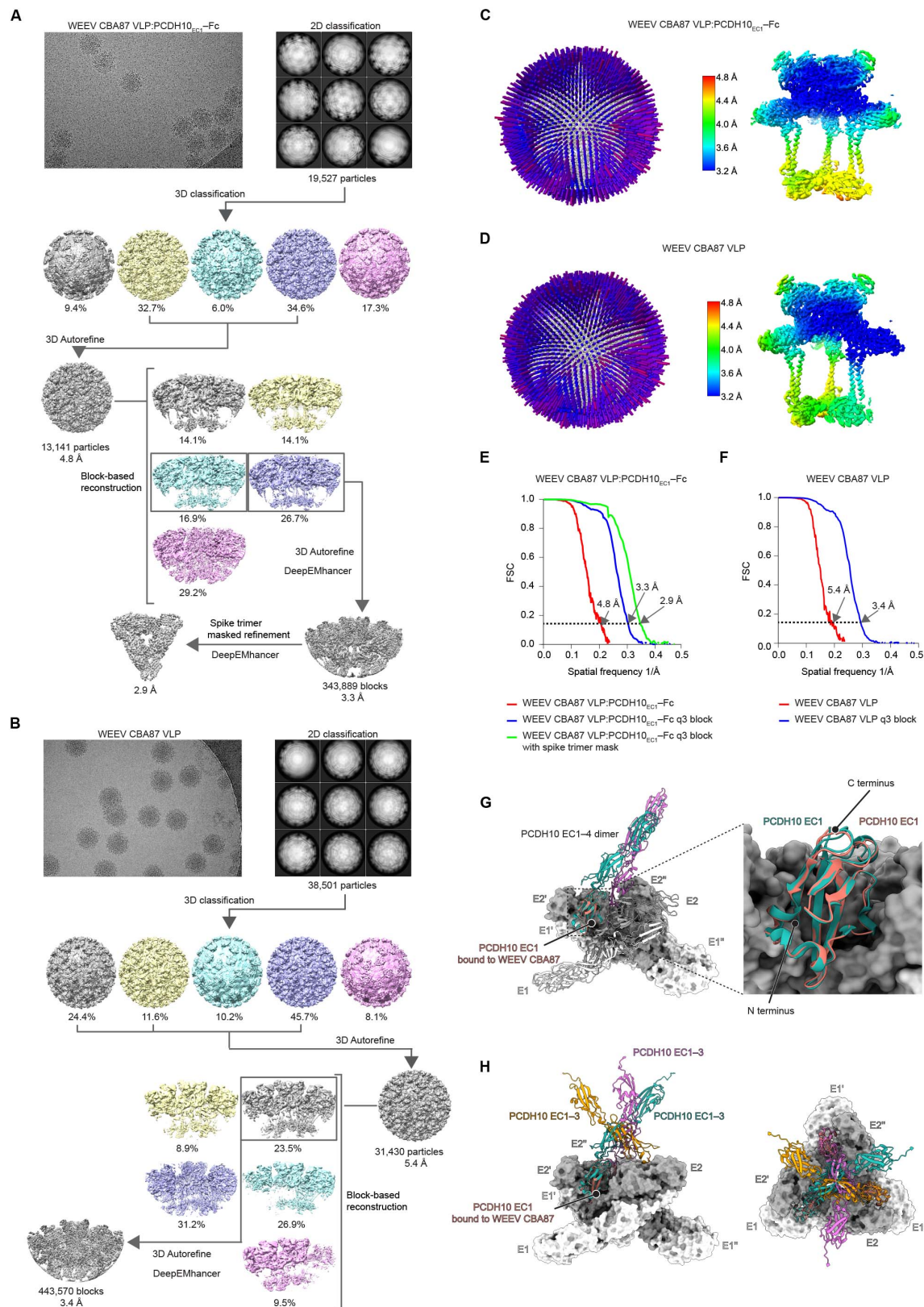
Supplementary Figure 3. Cryo-EM reconstructions of WEEV CBA87 VLPs alone or bound to human PCDH10$_{EC1}$–Fc. (A) Workflow used for cryo-EM data processing of WEEV CBA87

655   VLPs bound to human PCDH10$_{EC1}$–Fc. (B) Workflow used for cryo-EM data processing of
656   unliganded WEEV CBA87 VLPs. See Methods for additional details. (C and D) 3D representation
657   of particles angular distribution and local resolution map of the WEEV CBA87 VLP alone (D) or in
658   complex with PCDH10$_{EC1}$–Fc (C). (E and F) Fourier shell correlation curves of WEEV CBA87 VLP
659   alone (F) and bound to PCDH10$_{EC1}$–Fc (E) are shown, respectively. The threshold used to
660   estimate the resolution is 0.143. (G) Structural superimposition of the X-ray crystal structure of
661   PCDH10 EC1–4 homodimer (PDB ID: 6VFW)[14] with the WEEV CBA87:PCDH10$_{EC1}$–Fc complex
662   (left). (H) Superposition of the X-ray crystal structure of PCDH10 EC1–6 (PDB ID: 6VG4)[14] onto
663   the EC1 protomers bound to trimeric spike of WEEV CBA87. Occupancy of the three receptor-
664   binding sites on the trimer would result in showing steric hindrance between the EC2 repeat of
665   neighboring receptor molecules. The left panel shows a side view, and the right panel shows a
666   top view.
667
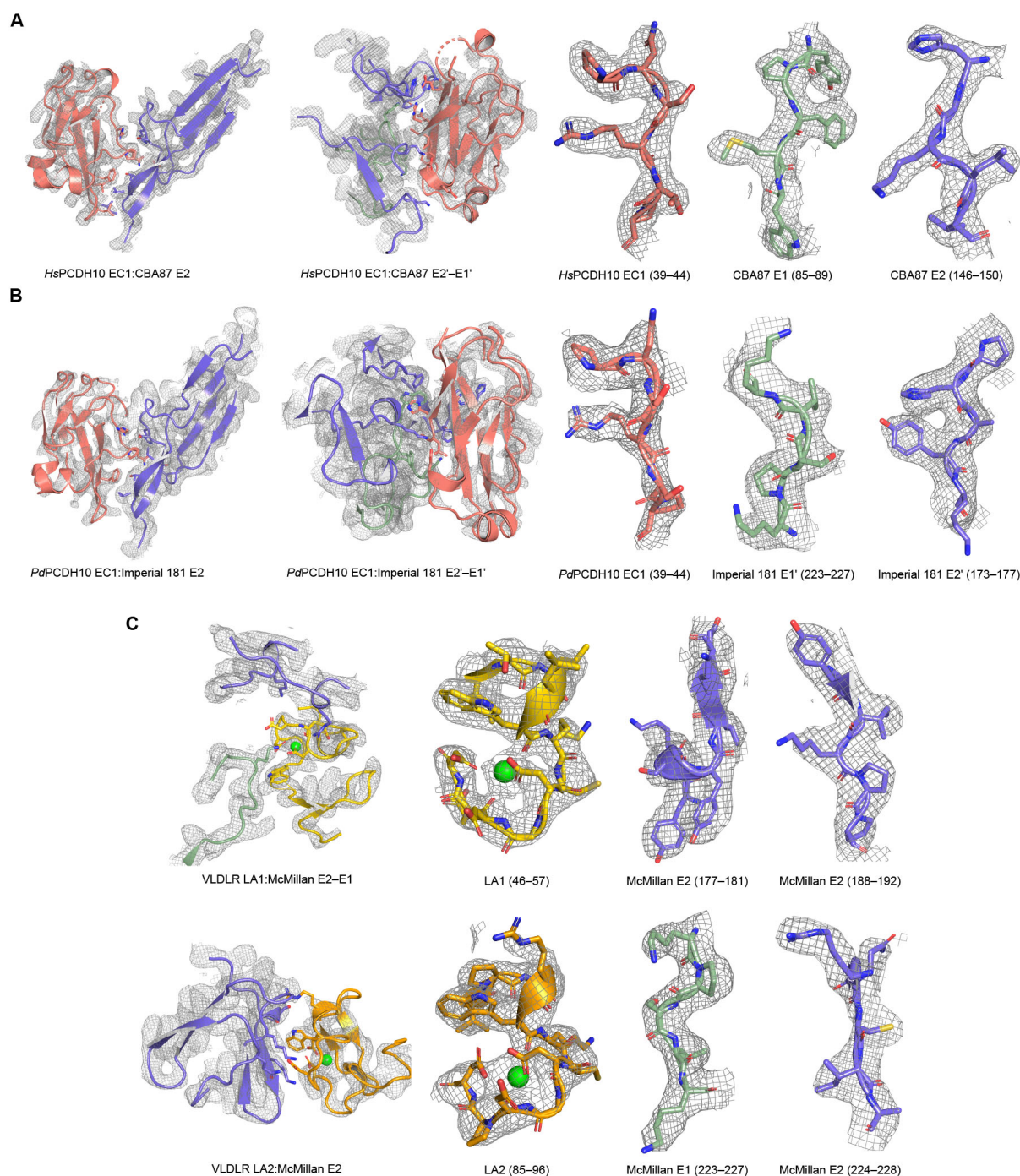
Supplementary Figure 4. Representative cryo-EM density maps of WEEV VLPs bound to *Hs*PCDH10, *Pd*PCDH10, and VLDLR. (A–C) Density maps of the indicated polypeptide segments from the following complexes: (A) WEEV CBA87 VLP bound to *Hs*PCDH10$_{EC1}$–Fc, (B) WEEV Imperial 181 VLP bound to *Pd*PCDH10$_{EC1}$–Fc, and (C) WEEV McMillan VLP bound to VLDLR$_{LBD}$–Fc.

A

Complex	BSA (Å²)	PDB ID
WEEV CBA87 human PCDH10 EC1	1,522	9DQV
WEEV Imperial 181 *Pd*PCDH10 EC1	1,540	9DQY
WEEV McMillan VLDLR LA1–LA2	746	9DQZ
WEEV McMillan Duck MXRA8	1,547	8DAN
WEEV McMillan Duck–D1–Mo–D2 MXRA8	1,611	8SQN
CHIKV Duck–D1–Mouse–D2 MXRA8	1,759	8EWF
CHIKV human MXRA8	2,012	6JO8
EEEV human VLDLR LA1	646	8UA4
EEEV human VLDLR LA1, LA2, and LA6	1,440	8UFB
SFV human VLDLR LA2	249	8UA8
SFV human VLDLR LA3	402	8IHP
VEEV human LDLRAD3	1,111	7FFF

Supplementary Figure 5. Comparison of contact surfaces for alphavirus E2 and E1 in receptor binding. (A) Buried surface area (BSA) calculations for the indicated complexes. (B) Surface rendering of the WEEV CBA87 spike protein trimer with one protomer of PCDH10 EC1 shown in ribbons. (C) Surface rendering of the WEEV McMillan spike protein with one protomer of chimeric Duck–D1–Mouse–D2 MXRA8 is shown in ribbons (PDB ID: 8SQN).[41] (D–F) Ribbon diagrams of WEEV E2–E1 heterodimers bound to surface-rendered PCDH10 EC1 or VLDLR LA1–LA2. E2 domains (A, B, and C) and E1 domains (DI-III) are indicated in different colors. Domain organization is shown as originally described by Voss et al.[55] FL: fusion loop.

Supplementary Figure 6. Sequence alignments of alphavirus E2–E1 glycoproteins and protocadherin EC1 repeats. (A and B) Sequence alignments of the E2 (A) and E1 (B) glycoproteins of WEEV CBA87 (GenBank: DQ432026.1), WEEV 71V658 (GenBank: NP_640331.1), WEEV McMillan (GenBank: DQ393792.1), EEEV FL91-469 (GenBank: Q4QXJ7.1), VEEV TC83 (GenBank: AAB02517.1), and SFV4 (GenBank: AKC01668.1). E2 and E1 residues that are with 4 Å of the indicated receptors in the structures are shown as indicated in the legend, and essential basic residues contacting LA repeats based on prior structural studies of LA repeat bound alphavirus spike proteins[17,19-22,37] are highlighted in green. Residues that are
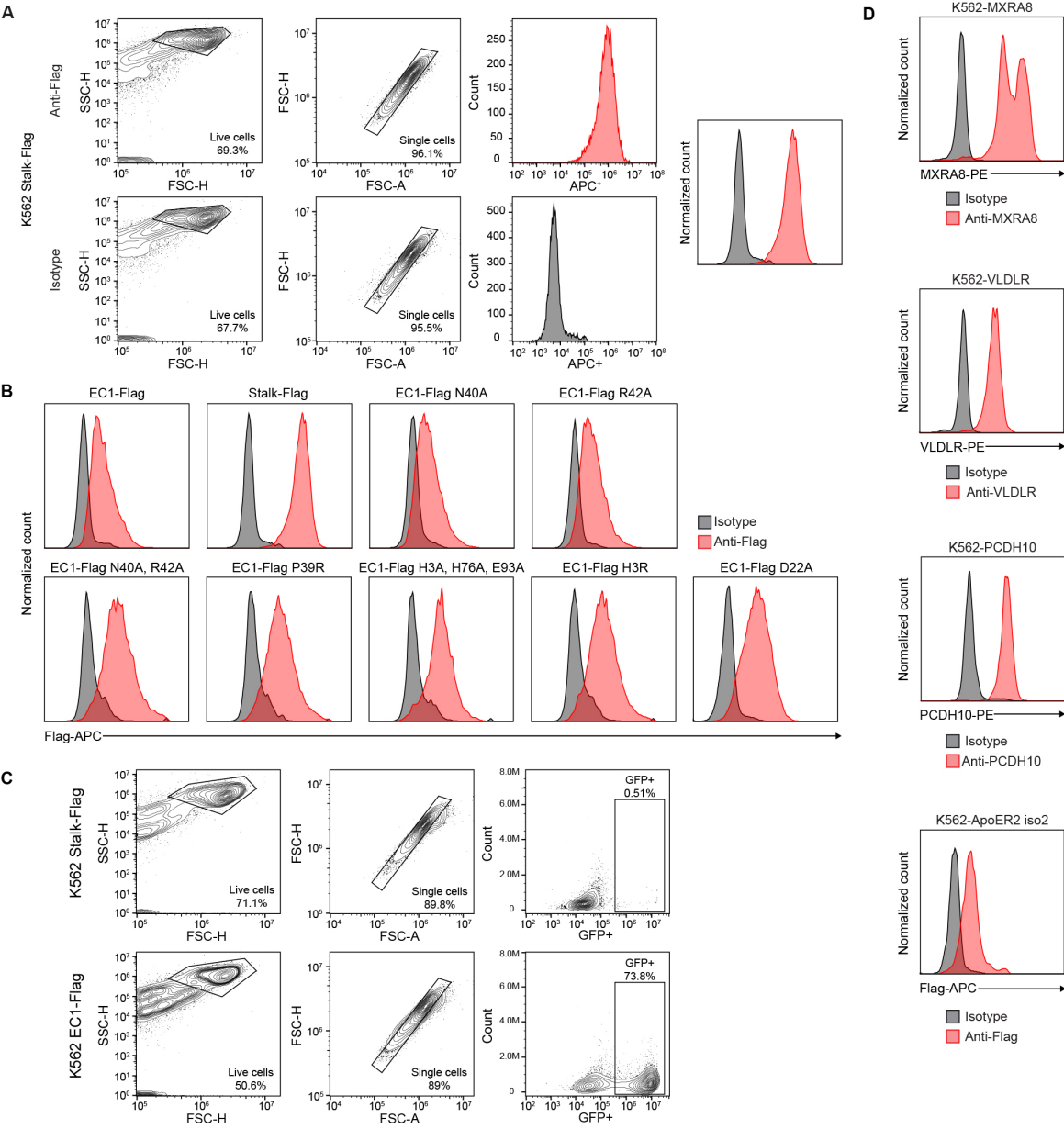
694 completely conserved in all aligned sequences have a red background. Boxed residues show
695 positions where a single majority residue or multiple chemically similar residues are found. Such
696 residues are in red. (C) Sequence alignments of PCDH10 EC1 orthologs of *H. sapiens* PCDH10
697 (GenBank: NP_116586.1); *M. musculus* PCDH10 (GenBank: NP_001091642.1); *E. caballus*
698 PCDH10 (GenBank: XP_023492316.1); *P. domesticus* PCDH10 (GenBank: XP_064272564.1);
699 *T. sirtalis* PCDH10 (GenBank: XP_013928164.1). (D) Sequence alignments of human PCDH10
700 EC1 with the EC1 repeats of other non-clustered δ2 protocadherins PCDH17 (GenBank:
701 NP_001035519.1) and PCDH19 (GenBank: NP_001171809.1). Residues that are completely
702 conserved have a gray background. Boxed residues highlight positions where a single majority
703 residue or multiple chemically similar residues could be identified. Such residues are highlighted
704 in pink. The panels were generated using ESPript 3.0.[54] PCDH10 residues that are with 4 Å of
705 the indicated spike proteins in the structures are shown as indicated in the legend.
706
707
708
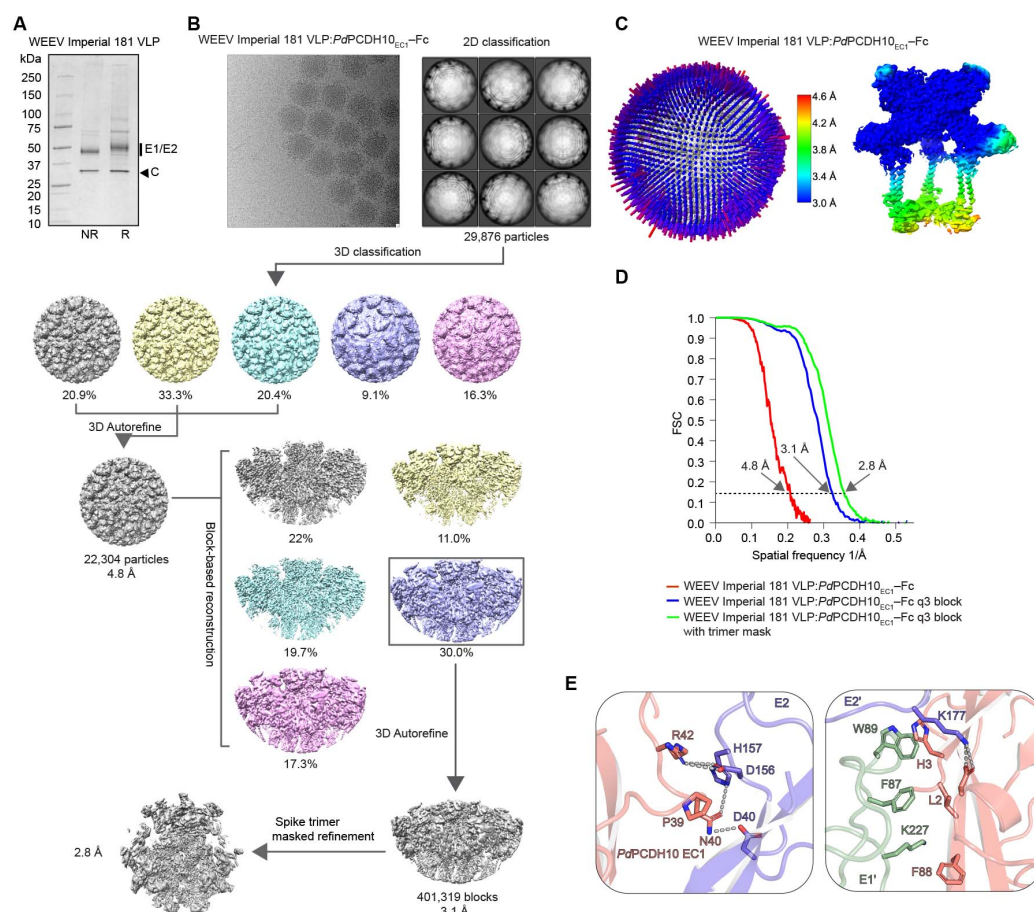
Supplementary Figure 7. Cryo-EM reconstruction of WEEV Imperial 181 VLP in complex with PdPCDH10$_{EC1}$–Fc. (A) Coomassie-stained SDS-PAGE gel of purified WEEV Imperial 181 VLPs. NR: non-reducing. R: reducing. (B) Workflow used for cryo-EM data processing of WEEV Imperial 181 VLPs bound to PdPCDH10$_{EC1}$–Fc. (C) 3D representation of particles angular distribution and local resolution maps of WEEV Imperial 181 VLP in complex with PdPCDH10$_{EC1}$–Fc. (D) Fourier shell correlation curves of WEEV Imperial 181 VLP in complex with PdPCDH10$_{EC1}$–Fc. The threshold used to estimate the resolution is 0.143. See Methods for additional details. (E) Interface between WEEV Imperial 181 E2–E1 or E2'–E1' and PdPCDH10 EC1. Residues that participate in interactions between WEEV Imperial 181 E2–E1 heterodimers and PdPCDH10 EC1 are indicated, with polar contacts shown as dashed lines.

723

724
725 **Supplementary Figure 8. Gating strategy and cell surface receptor staining.** (A) Example of
726 flow cytometry gating strategy used to quantify cells stained by antibodies. (B) Staining of K562
727 cell surface PCDH10 truncation constructs by APC-conjugated anti-Flag or isotype control
728 antibodies. (C) Example of flow cytometry gating strategy used to quantify cells expressing GFP
729 following infection by GFP-expressing RVPs. (D) Staining of K562 cells expressing the indicated
730 alphavirus receptors. PE: *R*-phycoerythrin.

731
732

A

WEEV spike protein residues that contact PCDH10

Lineage	WEEV strain or virus	E2 21	23	24	40	69	71	149	156	157	177	224	262	264	265	E1 87	89	227
A	California	H	A	P	D	Y	H	L	D	H	K	R	T	T	V	F	W	K
	Fleming	H	A	P	D	Y	H	L	D	H	K	K	T	T	F	F	W	K
	McMillan	H	A	P	D	Y	H	L	D	R	K	R	T	T	V	F	W	K
	Y62-33	H	A	P	D	Y	H	L	D	H	K	K	I	T	V	F	W	K
	CU71-CPA	H	A	P	D	Y	H	L	D	R	K	R	T	T	V	F	W	K
B1	BFS932	H	A	P	D	F	H	L	D	H	K	K	T	T	V	F	W	K
	BFS2005	H	A	P	D	F	H	L	D	H	K	K	T	T	V	F	W	K
	BFS09997	H	A	P	D	F	H	L	D	H	K	K	T	T	V	F	W	K
B2	EP6	H	T	P	D	F	H	L	D	H	K	K	T	T	I	F	W	K
	Montana-64	H	T	P	D	F	H	L	D	H	K	K	T	T	V	F	W	K
	71V1658	H	T	P	D	F	H	L	D	H	K	K	T	T	V	F	W	K
	85-452NM	H	T	P	D	F	H	L	D	H	K	K	T	T	V	F	W	K
	PV012357A	H	T	P	D	F	H	L	D	H	K	K	T	T	V	F	W	K
B3	R0PV00348A	H	T	P	D	F	H	**Q**	D	H	K	K	T	T	V	F	W	K
	R02PV003422B	H	T	P	D	F	H	**Q**	D	H	K	K	T	T	V	F	W	K
	Imperial 181	H	T	P	D	F	H	**Q**	D	H	K	K	T	T	V	F	W	K
C	CBA87	H	A	P	D	Y	H	L	D	H	K	K	T	T	V	F	W	K
	EQ1090	H	A	P	D	Y	H	L	D	H	K	K	T	T	V	F	W	K
	DILAVE218	H	A	P	D	Y	H	L	D	H	K	K	T	T	V	F	W	K
	Ar Enc MV	H	A	P	D	Y	H	L	D	H	K	K	T	T	V	F	W	K
	TR25717	H	A	P	D	Y	H	L	D	H	K	K	T	T	V	F	W	K
	AG80-646	H	V	P	D	L	Q	L	D	H	T	K	T	S	V	F	W	K
	Highlands J Virus	H	T	P	D	Y	Q	L	D	H	A	K	T	T	A	F	W	K

*Hs*PCDH10 ● contact residues at: 21, 69, 149, 156, 157, 177, 224, 262, 264, 265, 87, 89, 227
*Pd*PCDH10 ● contact residues at: 21, 23, 24, 40, 69, 156, 157, 177, 262, 264, 265, 87, 89, 227

● Contact residues

B

Lineage	WEEV strain or virus	McMillan VLDLR LA1 contact (site 1) E2 177	224	E1 227	McMillan VLDLR LA2 contact (site 2) E2 178	181	190	214	Fleming VLDLR likely contact (site 3) E2 81
A	California	K	R	K	S	**K**	K	Q	E
	Fleming	K	K	K	S	E	K	R	**K**
	McMillan	K	R	K	S	**K**	K	Q	E
	Y62-33	K	K	K	S	**K**	K	P	E
	CU71-CPA	K	R	K	S	**K**	K	Q	E
B1	BFS932	K	K	K	S	E	K	R	E
	BFS2005	K	K	K	S	E	K	R	D
	BFS09997	K	K	K	S	**K**	K	R	D
B2	EP6	K	K	K	S	**K**	K	R	E
	Montana-64	K	K	K	S	E	K	R	E
	71V1658	K	K	K	S	E	K	R	E
	Mn548	K	K	K	S	E	K	R	**K**
	85-452NM	K	K	K	S	E	K	R	E
	PV012357A	K	K	K	S	E	K	R	E
B3	R0PV00348A	K	K	K	S	E	K	R	E
	R02PV003422B	K	K	K	S	E	K	R	E
	Imperial 181	K	K	K	S	E	K	R	E
C	CBA87	K	K	K	S	E	K	R	E
	EQ1090	K	K	K	S	E	K	R	E
	DILAVE218	K	K	K	S	E	K	R	E
	Ar Enc MV	K	K	K	S	E	K	R	E
	TR25717	K	K	K	S	E	K	R	E
	AG80-646	T	K	K	S	E	K	R	D
	Highlands J virus	A	K	K	T	E	R	R	D

C

WEEV McMillan (Lineage A)

E2	Mortality (%)	MTD (days)	PCDH10	VLDLR/ApoER2
WT	100	4.8	Binding	Binding
K181E	70	6.7	Binding	No binding
Q214R	10	5	No binding	No binding
R224K	80	5	Binding	Binding

Expected effect: ▣ Binding ▢ No binding

Supplementary Figure 9. List of residues that contact receptors and summary of mouse virulence of McMillan mutants. (A) WEEV spike protein residues that contact *Hs*PCDH10 or *Pd*PCDH10 (< 4.0 Å). A key E2 polymorphic residue (Q149) is colored pink. (B) WEEV spike protein residues that contact VLDLR. Key polymorphic residues (E2 K181 and E2 K81) are colored in pink. (C) Effects of WEEV E2 McMillan mutations on mortality and mean time-to-death (MTD) when five-week-old female CD1 mice were inoculated 10^3 PFU subcutaneously in the left thigh, summarized from Mossel et al.[38] The expected effects of E2 mutations on PCDH10 or VLDLR/ApoER2 are based on the results of functional assays with McMillan RVPs shown in Figure 3G.
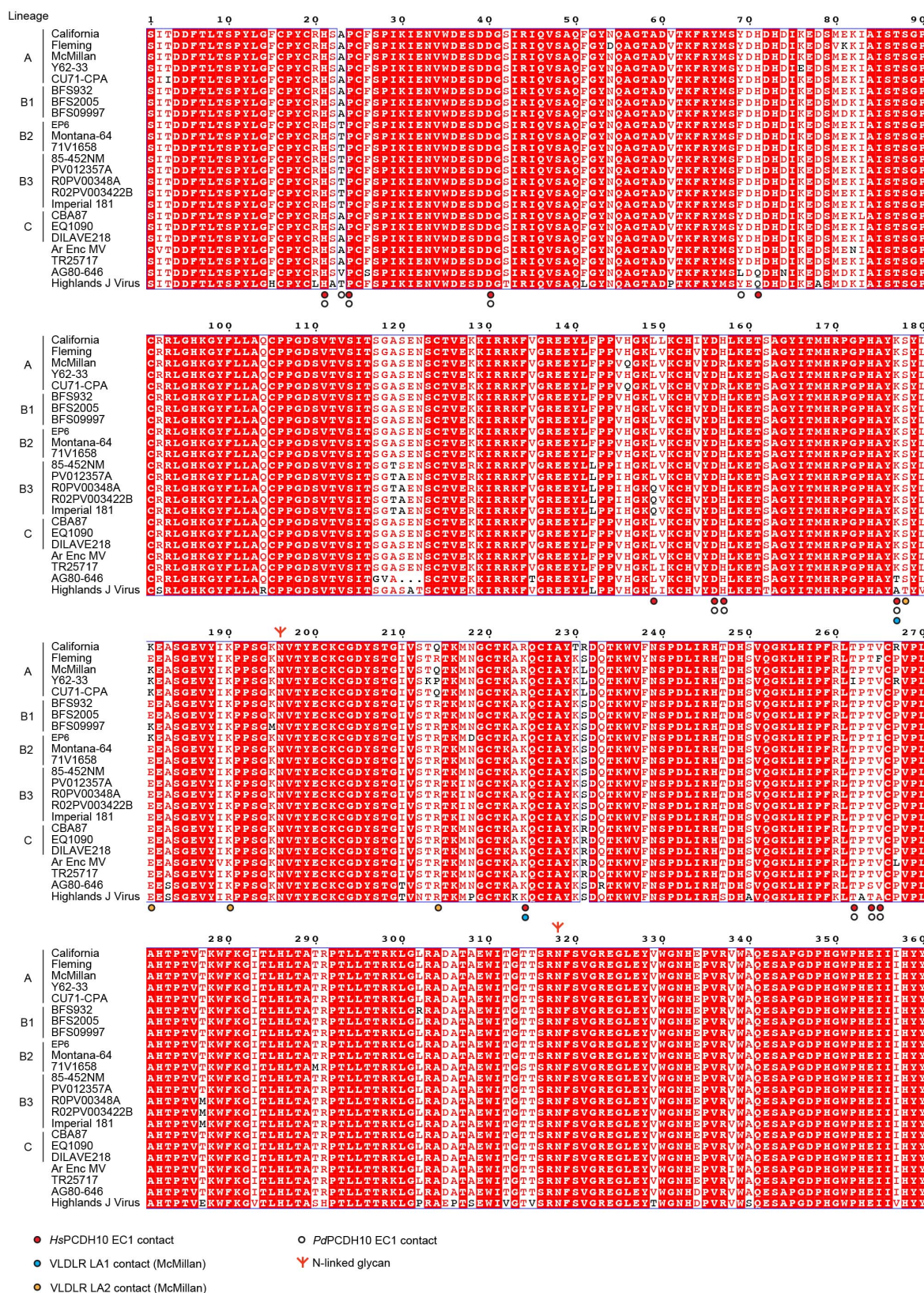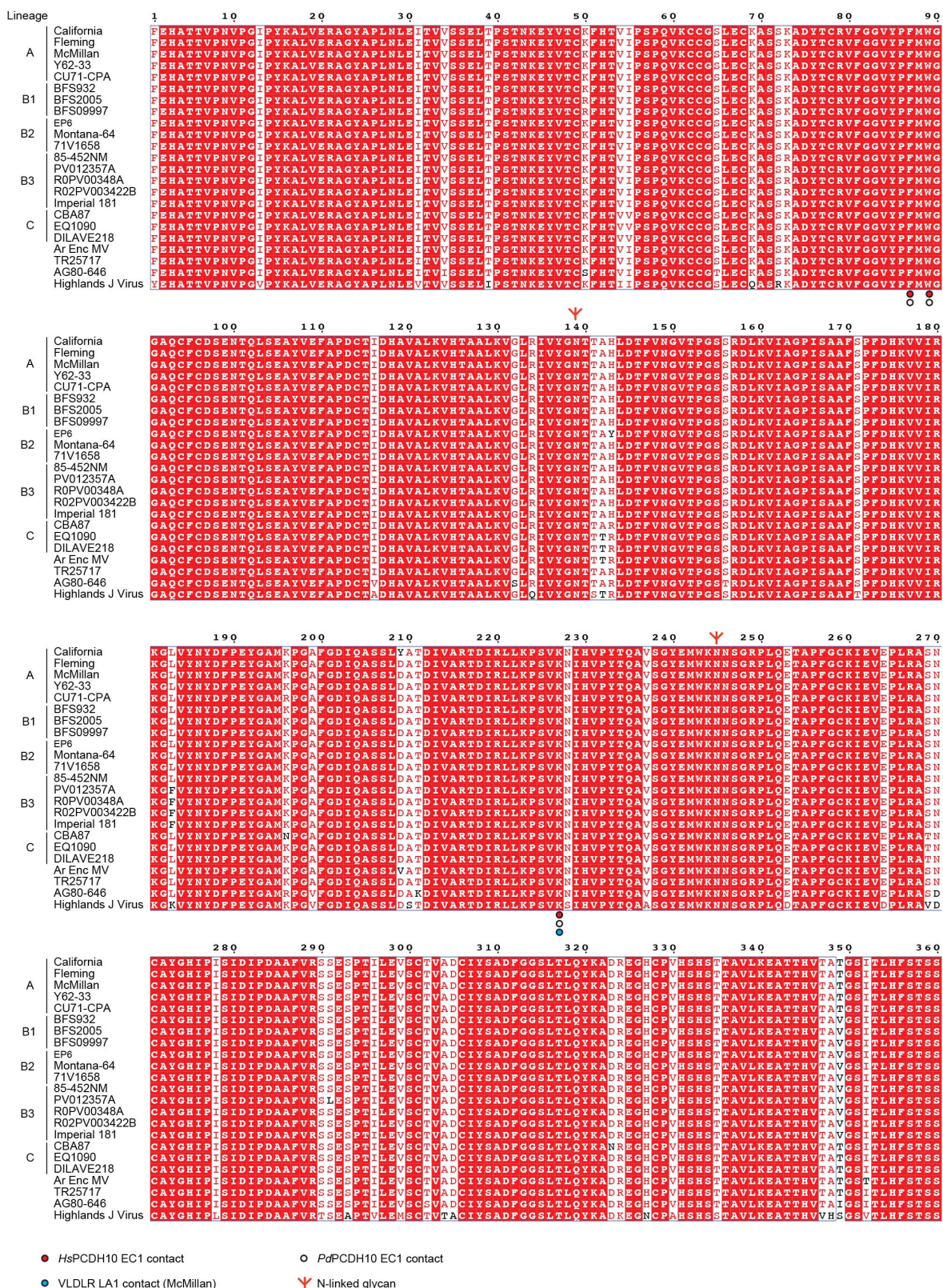
Supplementary Figure 10. Sequence alignments of different WEEV E2 glycoproteins. Sequence alignments of the E2 glycoproteins from different WEEV strains. The strain information

747 and accession numbers and are as follows: WEEV California (GenBank: KJ554965.1), WEEV
748 Fleming (GenBank: MN477208.1), WEEV McMillan (GenBank: DQ393792.1), WEEV Y62-33
749 (GenBank: KT844544.1), WEEV CU71-CPA (GenBank: KT844545.1), WEEV BFS932 (GenBank:
750 KJ554966.1), WEEV BFS2005 (GenBank: GQ287644.1), WEEV BFS09997 (GenBank:
751 KJ554974.1), WEEV EP6 (GenBank: KJ554967.1), WEEV Montana-64 (GenBank: GQ287643.1),
752 WEEV 71V1659 (GenBank: NP_640331.1), WEEV 85-452NM (GenBank: GQ287647.1), WEEV
753 PV012357A (GenBank: KJ554987.1), WEEV R0PV00348A (GenBank: KJ554991.1), WEEV
754 R02PV003422B (GenBank: KJ554990.1), WWEEV Imperial 181 (GenBank: GQ287641.1),
755 WEEV CBA87 (GenBank: DQ432026.1), WEEV EQ1090 (GenBank: PP544260.1), WEEV
756 DIAVE218 (GenBank: PP620644.1), WEEV Ar Enc MV (GenBank: KT844542), WEEV TR25717
757 (GenBank: KT844541), WEEV AG80-646 (GenBank: NC_075015), Highlands J virus 585-01
758 (GenBank: NC_012561.1). The Red background denotes residues that are completely conserved
759 in all sequences. Boxed residues highlight positions where a single majority residue or multiple
760 chemically similar residues are found. Such residues are highlighted in red. Receptor contact
761 residues and N-linked glycan sites are indicated as shown in the legend. The panels were
762 generated using ESPript 3.0.[54]
763
764
765
766

Supplementary Figure 11. Sequence alignments of different WEEV E1 glycoproteins. Sequence alignments of the E1 glycoproteins from different WEEV strains. The strain information

770 and accession numbers and are as follows: WEEV California (GenBank: KJ554965.1), WEEV
771 Fleming (GenBank: MN477208.1), WEEV McMillan (GenBank: DQ393792.1), WEEV Y62-33
772 (GenBank: KT844544.1), WEEV CU71-CPA (GenBank: KT844545.1), WEEV BFS932 (GenBank:
773 KJ554966.1), WEEV BFS2005 (GenBank: GQ287644.1), WEEV BFS09997 (GenBank:
774 KJ554974.1), WEEV EP6 (GenBank: KJ554967.1), WEEV Montana-64 (GenBank: GQ287643.1),
775 WEEV 71V1659 (GenBank: NP_640331.1), WEEV 85-452NM (GenBank: GQ287647.1), WEEV
776 PV012357A (GenBank: KJ554987.1), WEEV R0PV00348A (GenBank: KJ554991.1), WEEV
777 R02PV003422B (GenBank: KJ554990.1), WWEEV Imperial 181 (GenBank: GQ287641.1),
778 WEEV CBA87 (GenBank: DQ432026.1), WEEV EQ1090 (GenBank: PP544260.1), WEEV
779 DIAVE218 (GenBank: PP620644.1), WEEV Ar Enc MV (GenBank: KT844542), WEEV TR25717
780 (GenBank: KT844541), WEEV AG80-646 (GenBank: NC_075015), Highlands J virus virus 585-
781 01 (GenBank: NC_012561.1). Red background highlights residues completely conserved in all
782 sequences aligned. Boxed residues highlight positions where a single majority residue or multiple
783 chemically similar residues could be identified. Such residues are highlighted in red. Receptor
784 contact residues and N-linked glycan sites are indicated as shown in the legend. The panels were
785 generated using ESPript 3.0.[54]
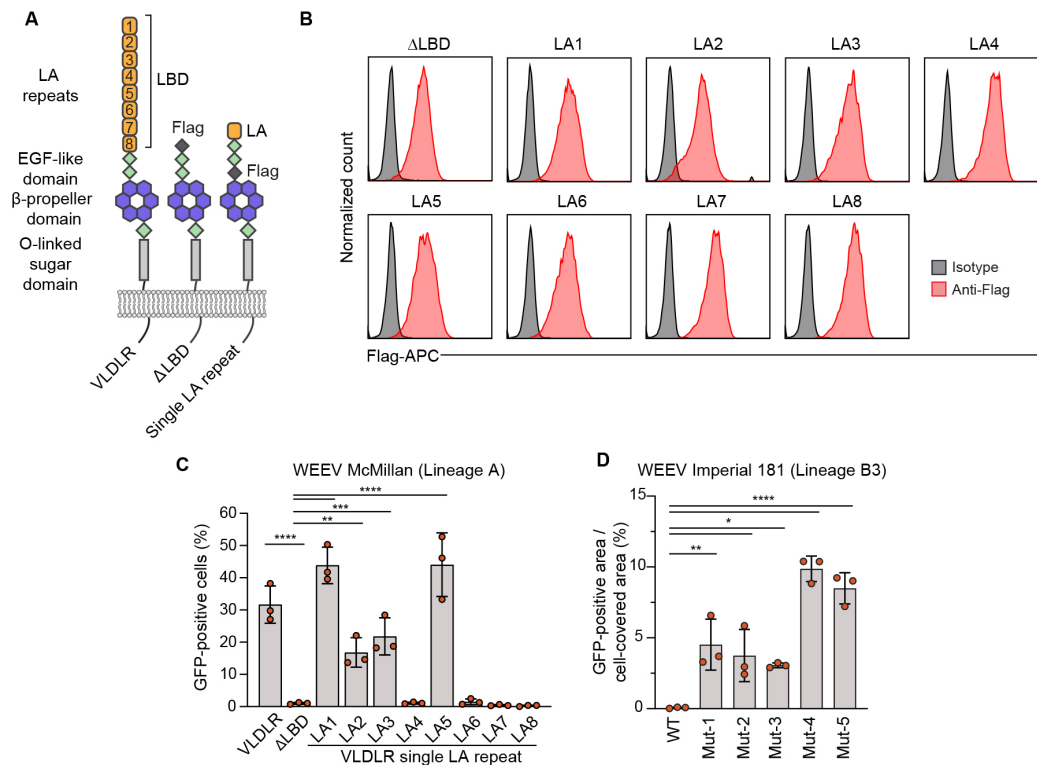
Supplementary Figure 12. WEEV McMillan LA repeat preferences and infectivity results with WEEV Imperial 181 RVP mutants. (A) Schematic diagrams of wild-type VLDLR and single LA repeat constructs. A ΔLBD construct in which the entire LBD is replaced by an N-terminal Flag tag is used as a negative control in experiments. (B) Staining of K562 cell surface VLDLR or Flag-tagged VLDLR truncation constructs by APC-conjugated anti-Flag or isotype control antibodies. (C) Infection of K562 cells stably expressing VLDLR, ΔLBD-Flag, or single LA repeat constructs by WEEV McMillan RVPs. Infection was quantified by flow cytometry. (D) Primary murine cortical neurons were infected with GFP-expressing wild-type or mutant WEEV Imperial 181 RVPs. Infection was monitored using a live cell imaging system (see Methods for additional information). Data are mean ± s.d. from three experiments performed in triplicates (n=3) (C, D). One-way ANOVA with Dunnett's multiple comparisons test, ****$P<0.0001$; ***$P<0.001$; **$P<0.01$ (C, D).

799
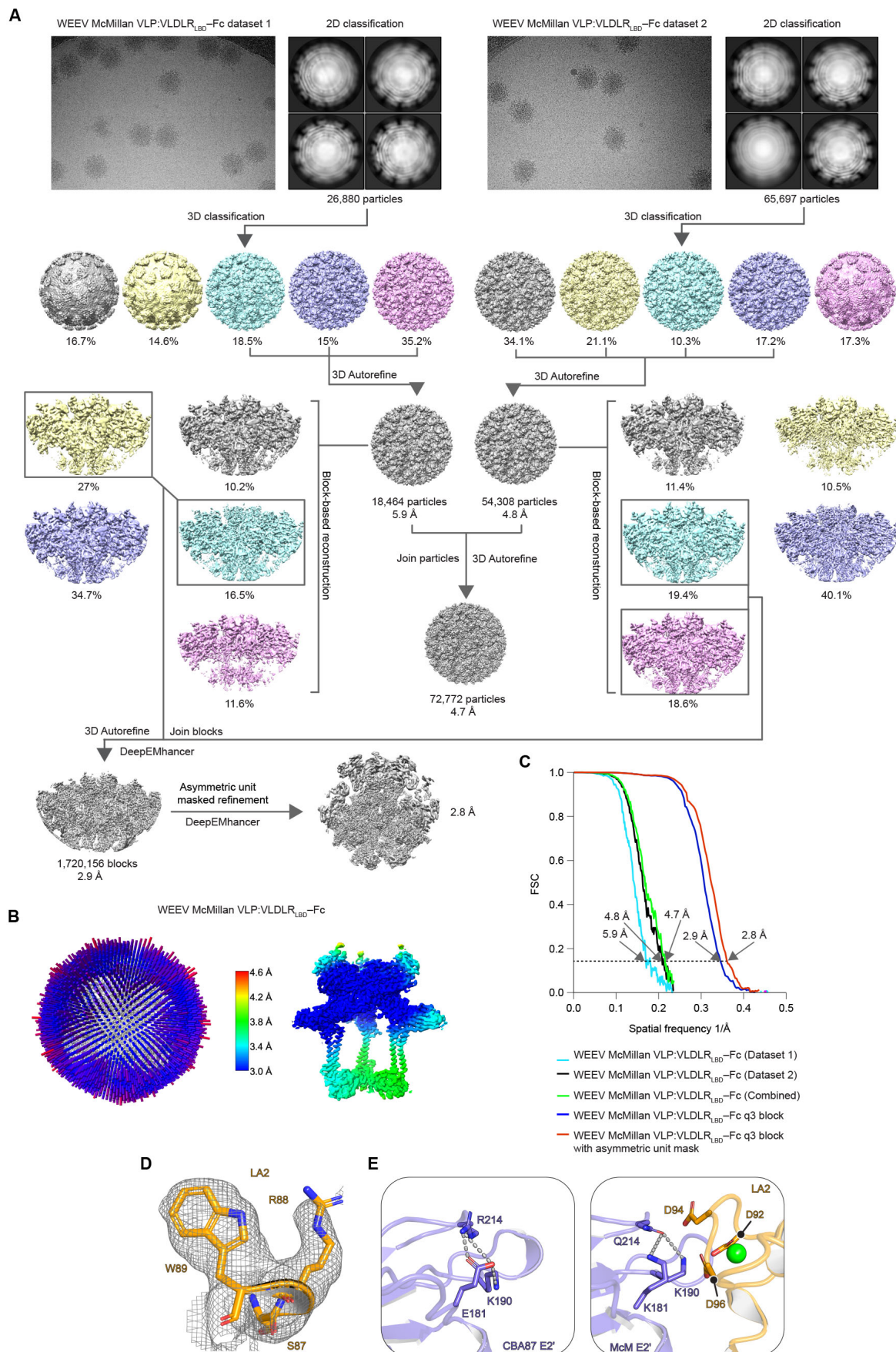
Supplementary Figure 13. Cryo-EM reconstruction of WEEV McMillan VLP in complex with VLDLR$_{LBD}$–Fc. (A) Workflow used for cryo-EM data processing of WEEV VLPs bound to VLDLR$_{LBD}$–Fc. (B) 3D representation of particles angular distribution and local resolution maps of WEEV McMillan VLP in complex with VLDLR$_{LBD}$–Fc. (C) Fourier shell correlation curves for WEEV McMillan VLP in complex with VLDLR$_{LBD}$–Fc. The threshold used to estimate the resolution is 0.143. See Methods for additional details. (D) Fitting of VLDLR LA2 into the LA repeat density of site 2. An elongated side chain density that could only be explained by an arginine (present in LA2) but not a serine (present in LA3) allowed for unambiguous identification of LA2 as the bound LA repeat at this site. (E) Comparison of WEEV McMillan E2 and CBA87 E2 near the key polymorphic E2 residues at positions 181 and 214. E2 E181 in CBA87 forms a salt bridge with E2 R214 (left panel). The Q214R substitution in McMillan E2 may locally destabilize E2 by positioning three basic residues (K181, K190, and R214) in close proximity (right panel).
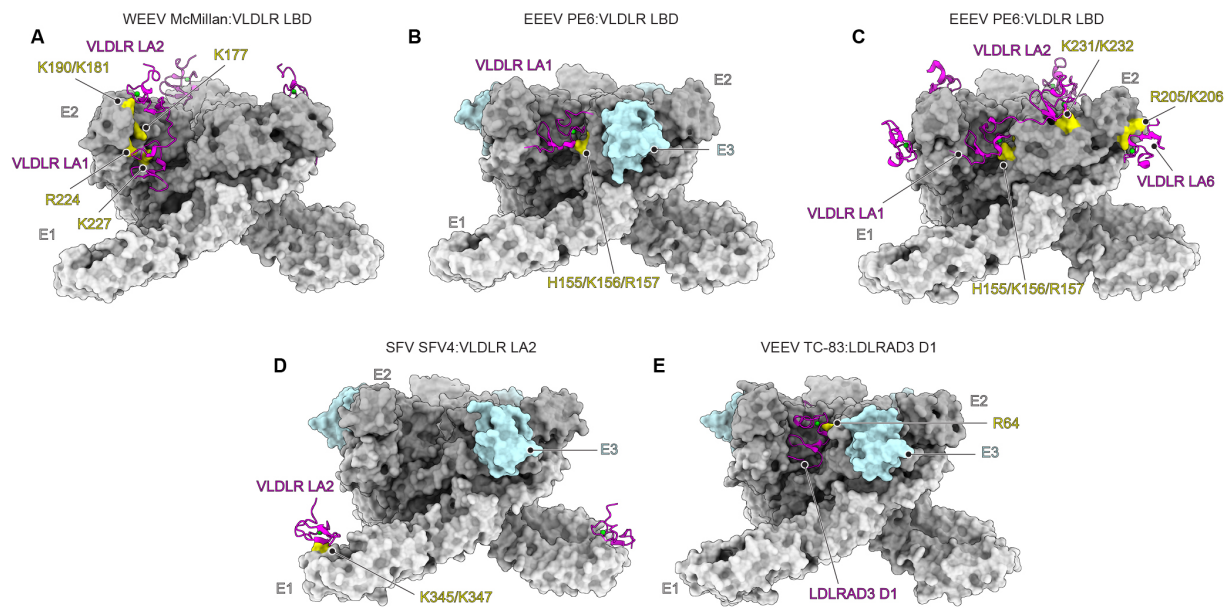
Supplementary Figure 14. Comparisons of alphavirus E2 and E1 bound to LA repeats.
(A–E) Alphavirus spike proteins are shown in a surface-rendered representation. The bound receptors are shown in ribbons. The LA repeat contact residues on WEEV McMillan, EEEV PE6 with retained E3 (B, PDB ID: 8UA4),[19] EEEV PE6 (C, PDB ID: 8UFB),[20] SFV SFV4 (D, PDB ID: 8UA8),[19] and VEEV TC-83 (E, PDB ID: 7FFF)[17] are colored in yellow. LA repeats are colored in magenta; E2–E1 glycoproteins are colored in different shade of gray; E3 is colored in light blue. LBD: ligand-binding domain. D1: domain 1.

Virus	Strain	Host	Year	Location	Passage history	GenBank accession number
WEEV	California	Horse	1930	San Joaquin Valley, California, USA	p (?), sm (27), C6 (1)	KJ554965
	Ar Enc MV	Horse	1933	Monte Veloz, Buenos Aires, Argentina		KT844542
	Fleming	Human	1938	California, USA	sm (5), v (3)	MN477208
	McMillan	Human	1941	Ontario, Canada	mp (2), sm (2), v (2), C6 (1)	GQ287640
	BFS932	Mosquito	1946	Bakersfield, California, USA	sm (1), v (1)	KJ554966
	EP-6	Mosquito	1950	Missouri, USA	ce (1), C6 (1)	KJ554967
	BFS1703	Mosquito	1953	Bakersfield, California, USA	sm (1), C6 (1)	KJ554968
	BFS2005	Mosquito	1954	Bakersfield, California, USA	de (1)	GQ287644
	CBA87	Horse	1958	Oncativo, Córdoba, Argentina	sm (14), bhk (2), v (2)	KT844543
	TR25717	Horse	1959	Guyana		KT844541
	B11		1961	USA	p (?), v (5), bhk (2)	DQ432027
	E1416	White-crowned sparrow	1961	Kern County, California, USA	bhk (4), C6 (1)	KJ554969
	Y62-33	Mosquito	1962	Russia		KT844544
	Montana-64	Horse	1967	Montana, USA	de (1), C6 (1)	GQ287643
	S8-122	Grey squirrel	1968	Butte County, California, USA	sm (1), C6 (1)	KJ554970
	CU71-CPA		1971	Cuba		KT844545
	BFS3060	Mosquito	1971	Butte County, California, USA	ce (1), sm (1), C6 (1)	KJ554972
	71V1658	Horse	1971	Oregon, USA	v (2), smb (1)	GQ287645
	TBT235	Tortoise	1971	Texas, USA	wc (1), de (1), sm (1), bhk (1), C6 (1)	KJ554971
	75V9291	Mosquito	1975	Wilkin City, Minnesota, USA	v (2), C6 (1)	KJ554973
	R7973	Human	1975	Larimer County, Colorado, USA		OQ184867
	BFS09997	Mosquito	1978	Kern County, California, USA	v (1), C6 (1)	KJ554974
	AG80-646	Mosquito	1980	Chaco, Argentina	v (2), sm (1)	GQ287646
	Mn520		1981	Manitoba, Canada	p (?), v (2)	DQ393793
	Kern5547	Mosquito	1983	Kern County, California, USA	v (1), C6 (1)	KJ554975
	CHLV53	Mosquito	1983	Riverside County, California, USA	v (1), C6 (1)	KJ554976
	Mn548		1984	Manitoba, Canada	p (?), v (2)	DQ393794
	85-452NM	Mosquito	1985	New Mexico, USA	sm (2), C6 (1)	GQ287647
	CHLV31	Mosquito	1985	Riverside County, California, USA		KT844547
	PV02808A	Mosquito	1990	Lubbock County, Texas, USA	v (1) or sm (1), C6 (1)	KJ554977
	CO921356	Mosquito	1992	Larimer City, Colorado, USA	v (1), C6 (1)	KJ554979

	IMPR441	Mosquito	1992	Imperial County, California, USA	sm (1), C6 (1)	KJ554978
	93A30	Mosquito	1993	Phoenix, Arizona, USA	v (1), C6 (1)	KJ554982
	93A79	Mosquito	1993	Yuma, Arizona, USA	v (1), C6 (1)	KJ554983
	SUYA140	Mosquito	1993	Sutter County, California, USA		KT844548
	CNTR34	Mosquito	1993	Contra Costa County, California, USA	v (1), C6 (1)	KJ554984
	SAC 74	Mosquito	1993	Sacramento County, California, USA		KT844549
	Lake43	Mosquito	1994	Lake County, California, USA	v (2), C6 (1)	KJ554985
	Kern87	Mosquito	1996	Kern County, California, USA		KT844550
	97-5067	Turkey	1996	Madera County, California, USA		KU978771
	98-2345	Emu	1997	USA		KU978772
	PV72102	Mosquito	1997	El Paso County, Texas, USA	v (1) or sm (1), C6 (1)	KJ554986
	PV012357 A	Mosquito	2001	El Paso County, Texas, USA	v (1) or sm (1), C6 (1)	KJ554987
	R02PV002 957B	Mosquito	2002	El Paso County, Texas, USA	v (1) or sm (1), C6 (1)	KJ554988
	R02PV001 807A	Mosquito	2002	El Paso County, Texas, USA	v (1) or sm (1), C6 (1)	KJ554989
	Imperial 181	Mosquito	2005	Imperial County, California, USA	v (2)	GQ287641
	R02PV003 422B	Mosquito	2005	El Paso County, Texas, USA	v (1) or sm (1), C6 (1)	KJ554990
	R0PV0038 4A	Mosquito	2005	El Paso County, Texas, USA	v (1) or sm (1), C6 (1)	KJ554991
	DILAVE070	Horse	2023	Paysandú, Uruguay		PP620641
	DILAVE158	Horse	2023	San José, Uruguay		PP620642
	DILAVE198	Horse	2023	San José, Uruguay		PP620643
	DILAVE218	Horse	2023	Paysandú, Uruguay		PP620644
	EQ1090	Horse	2023	Rio Grande do Sul, Brazil	not passaged	PP544260
	EQ1122	Horse	2023	Rio Grande do Sul, Brazil	not passaged	PP669618
	DILAVE236	Horse	2024	Rocha, Uruguay		PP620645
	DILAVE255	Horse	2024	San José, Uruguay		PP620646
	EQ237	Horse	2024	Rio Grande do Sul, Brazil	not passaged	PP669617
HJV	64A-1519	Horse	1964	Hillsborough County, Florida, USA	p (4), sm (1), v(1)	KT429021
	585-01	Red-tailed hawk	2001	Georgia, USA	v (1)	NC_012561
SFV	SFV4			Lab construct	Derived from molecular clone SFV3	AKC01668
EEEV	FL91-469	Mosquito	1991	Florida, USA	sm1, v3, bhk2	AY705241
MADV	267113	Human	2017	Darién, Panama		OR644805
SINV	360	Mosquito	2001	Queensland, Australia	C6 (1)	OL856089
CHIKV	37997	Mosquito	1983	Senegal	ap1, v2	AY726732

MAYV	BeH407	Human	1955	Brazil		MK573238
RRV	T48	Mosquito	1959	Australia	sm (6), C6 (1), v (1)	GQ433359
ONNV	UVRI0804	Human	2019	Uganda	v (1)	ON595759
GETV	AMM2021	Mosquito	1955	Malaysia	v (2), p (?)	MT121984
VEEV	TC83	Human	2017	Venezuela	Derived from VEEV strain TrD, passaged in the presence of SRI-34329	MZ399799

Supplementary Table 1. Strain information for viral sequences used in infectivity studies and phylogenetic analyses.
Passage numbers are in parentheses. "?" indicates unknown passage number. Abbreviations: mp: mouse; sm: suckling mouse; smb: suckling mouse brain; v: Vero cells; bhk: baby hamster kidney cells; wc: wet chicks; de: duck embryonic fibroblasts; ce: chick embryonic fibroblasts; C6: C6/36 (*Aedes albopictus*) cells; ehe: embryonated hen's eggs; gp: guinea pig; p: unknown media.

829 **Supplementary Table 2. Cryo-EM data collection and validation statistics**.

	WEEV CBA87 VLP: Human PCDH10$_{EC1}$–Fc	WEEV Imperial 181 VLP: Sparrow PCDH10$_{EC1}$–Fc	WEEV McMillan VLP: VLDLR$_{LBD}$–Fc		WEEV CBA87 VLP unliganded
			Dataset 1	Dataset 2	
Magnification	81,000	130,000	81,000	81,000	81,000
Voltage (kV)	300	300	300	300	300
Pixel Size (Å)	1.06	0.94	1.06	1.06	1.06
Electron dose (e/Å^2)	52.2	50	53.3	54.4	53.9
Defocus range (µm)	-0.6 to -1.8	-0.8 to -1.8	-0.8 to -1.8	0.8 to -1.8	-0.6 to -1.8
VLP reconstruction					
Initial particles	22,075	38,927	34,210	95,449	43,025
Final particles	13,141	22,304	18,464	54,308	31,430
Symmetry imposed		Icosahedral symmetry			
FSC threshold	0.143	0.143	0.143		0.143
Map resolution (Å)	4.8	4.8	5.9	4.8	5.4
Block-based reconstruction					
			Dataset 1	Dataset 2	
Initial Blocks	788,460	1,338,240	1,107,840	3,258,480	1,885,800
Final Blocks	343,889	401,369	1,720,156		443,570
Symmetry imposed	C1	C1	C1		C1
FSC threshold	0.143	0.143	0.143		0.143
	q3 block / spike trimer	spike trimer	q3 block / spike trimer		q3 block
Map resolution (Å)	3.3 / 2.9	2.8	2.9 / 2.8		3.4
Model refinement and validation					
Initial model used		AlphaFold2			
R.m.s deviations					
Bonds lengths (Å)	0.004	0.003	0.006		0.004
Bonds angles (º)	0.730	0.616	0.735		0.765
Validation					
Clashscore	15	8	13		16
Favored (%)	93	95	95		93
Allowed (%)	7	5	5		7
Disallowed (%)	0	0	0		0

830
831

832 **Methods**

833 **Cell lines and viruses**

834 All cell lines used in this study are listed in the key resources table. HEK 293T (human kidney

835 epithelial, ATCC CRL-11268), Vero E6 (*Cercopithecus aethiops* kidney epithelial, ATCC CRL-

836 1586) were maintained in Dulbecco's modified Eagle's medium (DMEM, Gibco) supplemented

837 with 10% (v/v) fetal bovine serum (FBS) and 25 mM HEPES (Thermo Fisher Scientific). K562

838 (human chronic myelogenous leukemia, ATCC CCL-243) cells were maintained in RPMI1640

839 (Thermo Fisher Scientific) supplemented with 10% (v/v) FBS, 25 mM HEPES, and 1% (v/v)

840 penicillin-streptomycin. Expi293F cells (Thermo Fisher Scientific Cat#: A14527) were maintained

841 in Expi293 Expression Medium (Thermo Fisher Scientific). Cell lines were not authenticated.

842 Absence of mycoplasma is confirmed through routine mycoplasma test using e-Myco PCR

843 detection kit (Bulldog Bio Cat#: 25234).

844

845 **Production and purification of virus-like particles**

846 The genes encoding the structural polyprotein (capsid-E3-E2-(6K/TF)-E1) of WEEV strains

847 CBA87 (GenBank: DQ432026.1), McMillan (GenBank: DQ393792.1), and Imperial 181

848 (GenBank: GQ287641.1) with capsid K67N mutation used to improve the yield of VLP

849 production[30] were separately cloned into the pVRC vector. We also produced EEEV VLPs using

850 a previously described vector that encodes the structural polyprotein of EEEV strain PE6

851 (GenBank: AAU95735.1) with capsid mutation K67N.[30] Expi293F[TM] (Thermo Fisher Scientific)

852 cells were cultured at 37°C with 5% CO_2 in the Expi293[TM] expression medium. We transfected

853 Expi293F[TM] cells with pVRC vectors encoding WEEV structural polyproteins using

854 ExpiFectamine[TM] 293 Transfection Kit (Thermo Fisher Scientific) according to the manufacturer's

855 instructions. We collected culture supernatant 5 d post-transfection and pelleted cells by

856 centrifugation at 3,000 g for 20 min. The clarified supernatant was ultracentrifuged with a sucrose

857 cushion consisting of 5 ml of 35% (w/v) sucrose and 5 ml of 70% (w/v) sucrose at 110,000 x *g* for

858   5 h in a Beckman SW28Ti rotor at 4°C. The VLPs were pooled from the interface of the 35% (w/v)

859   and 70% (w/v) sucrose cushions, then buffer exchanged to lower the sucrose concentration to

860   less than 20% (v/v) at a volume of 1 ml using a 100-kDa Amicon filter (Sigma). The VLPs were

861   loaded onto a 20%–70% (v/v) continuous sucrose density gradient and centrifuged for 1.5 h in a

862   Beckman SW41 rotor at 210,000 x g at 4°C. The VLP band was collected and exchanged into

863   Dulbecco's Phosphate Buffered Saline (DPBS, Thermo Fisher Scientific Cat#: 14190-144) using

864   a 100-kDa Amicon filter. We confirmed integrity and purity of VLPs using SDS-PAGE (Figures

865   S2A and S7A).

866

867   **Expression and purification of recombinant proteins**

868   The genes encoding the EC1 domain of human PCDH10 (residues 19-122, GenBank

869   NP_116586.1),[10] the human VLDLR LBD (residues 31–355, GenBank NP_003374.3),[39] or the

870   human MXRA8 ectodomain (residues 20–337, GenBank NP_001269511.1)[39] with the human

871   IgG1 Fc region at their C terminal were separately cloned into the pVRC vector. We subcloned

872   the EC1 domain of *P. domesticus* PCDH10 (residues 19-122, GenBank XP_064272571.1) into

873   the same pVRC vector, provided by A. Schmidt.[66] To purify PCDH10$_{EC1}$–Fc and MXRA8$_{ect}$–Fc,

874   we transfected Expi293F^{TM} cells with plasmids encoding the fusion proteins using

875   ExpiFectamine^{TM} 293 Transfection Kit (Thermo Fisher Scientific Cat#: A14525) according to the

876   manufacturer's instructions. Supernatants were collected 5 d post-transfection, centrifuged at

877   4,000 g for 30 min and purified with MabSelect^{TM} PrismA protein A affinity resin (Cytiva Cat#:

878   17549801) using the manufacturer's protocol. The proteins were further purified by size-exclusion

879   chromatography on a Superdex 200 increase 10/300 column (Cytiva). Proteins were stored in

880   Tris Buffered Saline (TBS) (20 mM Tris, 150 mM NaCl in water, pH 7.5).

881   To purify VLDLR$_{LBD}$–Fc, we co-transfected Expi293F cells with the pVRC vector encoding

882   VLDLR$_{LBD}$–Fc and a pCAGGS vector encoding the chaperon receptor-associated protein (RAP,

883   residues 1-353, GenBank NP_002328). Supernatants were collected 5 d post-transfection and

884 purified with MabSelect^{TM} PrismA protein A affinity resin. We separated the VLDLR$_{LBD}$–Fc from

885 RAP on the column by washing the column with 300 volumes of 10 mM EDTA in TBS overnight.

886 Then VLDLR$_{LBD}$–Fc was refolded on the column by washing with 100 column volumes of 2 mM

887 CaCl$_2$ in TBS and eluted using the manufacturer's protocol. The proteins were concentrated and

888 further purified by size-exclusion chromatography on a Superdex 200 increase 10/300 GL column.

889 RAP was stored in TBS and VLDLR$_{LBD}$–Fc was stored in TBS containing 2 mM CaCl$_2$.

890 The genes encoding the EC1 domain of human PCDH10 (residues 19-122, GenBank

891 NP_116586.1) were cloned into a pVRC vector with a C-terminal twin-strep tag for purification.

892 We transfected Expi293F^{TM} cells with plasmid using ExpiFectamine^{TM} 293 Transfection Kit

893 according to the manufacturer's instructions. After centrifugation at 4,000 g for 30 min,

894 supernatants were incubated with Strep-Tactin$^{®}$ XT Sepharose resin (IBA Lifesciences) for 1 h at

895 4 ˚C. The beads were then washed using TBS, and the bound proteins were eluted using 50 mM

896 biotin in TBS. The proteins were further purified by size-exclusion chromatography on a Superdex

897 200 increase 10/300 column equilibrated with TBS.

898

899 **Biolayer interferometry binding assays**

900 We performed biolayer interferometry experiments with an Octet RED96e (Sartorius) and

901 analyzed data using ForteBio Data Analysis HT version 12.0.1.55 software. The anti-WEEV E

902 protein monoclonal antibody SKW11 (a gift from M. Sutton and M. Roederer)[56] was loaded onto

903 Anti-Human IgG Fc Capture (AHC) Biosensors (Sartorius Cat#: 18-5063) at a concentration of

904 250 nM in kinetic buffer (TBS supplemented with 2 mM CaCl$_2$, 0.1% (w/v) BSA and 0.01% Tween)

905 for 600 s. After a baseline measurement in kinetic buffer for 60s, tips were dipped into wells

906 containing 1 μM WEEV CBA87 VLPs for 1 h. The signal was then allowed to equilibrate for an

907 another 1 h in kinetic buffer. The tips were washed with the kinetic buffer for 60 s to obtain a

908 baseline reading, then the biosensors were dipped into wells containing the serial dilutions of

909 human PCDH10$_{EC1}$–twin-strep (concentration range of 10 μM to 312.5 nM) in kinetic buffer for

910   900 s. Finally, a 300 s dissociation in kinetic buffer was performed. Data analysis was performed

911   using a standard 1:1 binding model.

912

913   **ELISA**

914   Apparent affinities of *Hs*PCDH10 EC1–Fc and *Pd*PCDH10$_{EC1}$–Fc for CBA87, McMillan and

915   Imperial 181 VLPs were also separately determined by ELISA. 200 ng VLPs were immobilized on

916   ELISA MaxiSorp plates (Thermo Scientific Cat#: 439454) overnight at 4 ˚C. The coated plates

917   were blocked by PBS supplemented with 3% (w/v) BSA for 1 h at room temperature, then were

918   washed five times with PBS. Serial dilutions of *Hs*PCDH10$_{EC1}$–Fc or *Pd*PCDH10$_{EC1}$–Fc proteins

919   were prepared and added to plates and incubated for 1 h at room temperature. After incubation

920   with Fc-fusion proteins, the plates were washed five times with PBS, and then 100 µl per well of

921   horseradish-peroxidase-conjugated anti-Human IgG (Sigma Cat#: A0170) diluted at ratio of

922   1:20,000 in PBS supplemented with 3% BSA were added for incubation for 1 h at room

923   temperature. The plates were washed five times with PBS, then incubated with 100 µl per well of

924   1-step TMB ELISA solution for 3 min at room temperature in the dark and the reactions were

925   stopped by addition of 100 µl per well of 2 N sulfuric acid. Absorbance was read at an optical

926   density of 450 nm using BioTek multi-mode reader. EEEV VLPs were used as negative controls

927   in experiments.

928

929   **Truncation and mutagenesis, and stable cell line generation**

930   cDNA encoding human PCDH10 (GenBank NM_032961.3), human VLDLR (GenBank

931   NP_003374.3), human MXRA8 (GenBank NM_032348.3), human ApoER2 isoform 2 (GenBank

932   NM_004631.5), *P. domesticus* PCDH10, *P. domesticus* MXRA8, *E. caballus* PCDH10 (GenBank

933   XM_023636548.1), *T. sirtalis* PCDH10 (GenBank XM_014072689.1), *M. musculus* PCDH10

934   (GenBank: NP_001091640.1) were cloned into a lentiGuide-Puro (Addgene #52963) expression

935   vector as previously described.[10] Non-human sequences were codon optimized for expression in

936   human cells.

937   For the single PCDH10 EC1 construct, residues 19-690 in the PCDH10 precursor protein

938   were replaced with residues 19-122 and adding a Flag tag (DYKDDDDK) between S696 and

939   G697. Point mutations of contact residues in EC1 were generated using site-directed

940   mutagenesis on the background of the single PCDH10 EC1 construct. For PCDH10 stalk-Flag,

941   residues 19-690 in the precursor protein sequence were removed and a Flag tag (DYKDDDDK)

942   was added between S696 and G697. VLDLR truncation constructs were previously described.[19]

943   Wild-type and mutant PCDH10 and VLDLR constructs were cloned into a lentiGuide-Puro

944   (Addgene #52963) expression vector.

945   To generate lentiviruses for stable transduction, lentiGuide-Puro plasmids containing the

946   transgene were co-transfected with psPAX2 (Addgene #12260) and PMD2.G (Addgene #12259)

947   at a ratio of 3:2:1 into HEK 293T cells using Lipofectamine 3000 (Thermo Fisher Scientific).

948   Lentiviruses were harvested 2 d post-transfection and used to transduce K562 cells. Successfully

949   transduced K562 cells were selected for using puromycin at 2 μg ml^{-1}. Cell lines were confirmed

950   to express the constructs of interest at the plasma membrane by cell surface antibody staining

951   (Figure S8). Antibodies are listed in the key resources table.

952

953   **Reporter virus particle generation**

954   RVPs were generated as previously described[39] using a dual vector system: a modified pRR64

955   Ross River virus replicon[67] provided by R. Kuhn (Purdue University) (the SP6 promoter is replaced

956   with a CMV promoter, the E3-E2-6K/TF-E1 sequence is replaced with a turbo GFP reporter

957   preceded by a porcine teschovirus-1 2A self-cleaving peptide), and a pCAGGS vector expressing

958   heterologous WEEV E3-E2-6K/TF-E1 proteins. The two vector were co-transfected into HEK

959   293T cells using Lipofectamine 3000 (Thermo Fisher). 4-6 h post-transfection, we replaced media

960   with Opti-MEM (Thermo Fisher) supplemented with 5% (v/v) FBS, 25 mM HEPES, and 5 mM

961 sodium butyrate. We harvested supernatant 2 d post-transfection, centrifuged supernatant at

962 4,000 rpm for 5 min, filtered using a 0.45 μm filter, and froze aliquots at −80 °C for storage.

963 WEEV E3-E2-6K/TF-E1 coding sequences cloned into the pCAGGS vector include: strain

964 71V1658 (GenBank NC_003908.1), strain Fleming (GenBank MN477208.1), strain McMillan

965 (GenBank GQ287640.1), strain Imperial 181 (GenBank GQ287641.1), strain CBA87 (GenBank

966 KT844543.1), strain BFS09997 (GenBank KJ554974.1), strain EP6 (GenBank KJ554967.1),

967 strain AG80-646 (GenBank NC_075015.1), strain TR25717 (GenBank KT844541.1), strain

968 EQ1090 (GenBank PP544260.1), strain DILAVE218 (GenBank PP620644.1). For HJV, strain

969 585-01 (GenBank NC_012561.1) was used. Mutant E3-E2-6K/TF-E1 sequences were generated

970 using site-directed mutagenesis.

971 Titration of RVPs for MOI calculation was performed on Vero E6 cells seeded in a 96-well

972 plate using a serial tenfold dilution of the RVP stocks. 24 h post-infection, numbers of GFP-

973 positive cells were counted and used to calculate RVP titer as infectious unit per milliliter (IU ml^{-}

974 ^{1}), assuming that at high dilution factors, each GFP-positive cell is infected with one RVP given

975 that RVPs only infect cells for one cycle.

976

977 **Reporter virus particle entry assays**

978 We incubated transduced K562 cells with RVPs. 24 h post-infection, cells were harvested,

979 washed twice with PBS, and fixed in PBS containing 2% (v/v) formalin. GFP expression was

980 measured by FACS using an iQue3 Screener PLUS (Intellicyt) with IntelliCyt ForeCyt Standard

981 Edition version 8.1.7524 (Sartorius) software. An example of the flow cytometry gating scheme

982 used to quantify GFP-expressing RVP infection is provided in Figure S8.

983 For assessment of efficiency of receptor recognition, RVPs were titrated on K562 cells

984 expressing cognate receptors in a twofold dilution series, with multiplicity of infection (MOI)

985 calculated based on titers measured on Vero E6 cells.

986

Mouse cortical neuron culture and infection

Embryonic day 17 mouse cortical neurons were purchased (Thermo Fisher Scientific Cat#: A15586) and cultured according to the manufacturer's protocol with modifications. In brief, neurons were thawed and plated on 96 well plates coated with Poly-D-Lysine at 4.5 µg cm^{-2} at 40,000 neurons per well, in neurobasal medium (Thermo Fisher Scientific Cat#: 21103) supplemented with 0.5 mM Glutamax (Thermo Fisher Scientific Cat#: 35050), 2% (v/v) B-27 (Thermo Fisher Scientific Cat#: 17504), and 10 µM Y-27632 (Stemcell Technologies Cat#: 72302). 24 h post-plating, a full medium change was performed to remove Y-27632. Half medium change was performed every third day until infection. Neurons were infected with WEEV Imperial 181 wild-type or mutant RVPs at an MOI of 2 in the presence or absence of a control IgG (316 µg ml^{-1}), $PCDH10_{EC1}$–Fc (216 µg ml^{-1}), or RAP (100 µg ml^{-1}). 8 h post-infection, neurons were scanned using the Incucyte S3 Live Cell Imaging system (Sartorius) with Incucyte S3 Software version 2023A Rev2 (Sartorius) using a 20× objective. GFP-positive neurons were scored as cells with a threshold signal greater than 3 green calibrated units (GCU) above background, using a Surface Fit background subtraction method. The neuronal cell body area in each image was obtained by analyzing phase-contrast images using the Incucyte S3 Software (version 2023B). To calculate the percentage of positive cells, at the time point of 8 h post-infection, the area of GFP signal above background was divided by the total area covered by neuronal cell bodies and was multiplied by 100. Relative infection was calculated as follows: Relative infection (%) in the presence of recombinant proteins = (Percentage of GFP-positive cells in the presence of recombinant proteins) / (Percentage of GFP-positive cells under mock treatment) × 100.

Cryo-EM sample preparation and data collection

We first mixed 3 µl of WEEV VLPs (with structural polyprotein sequence derived from strain CBA87 [GenBank: DQ432026.1]) at a concentration of 3.0 mg ml^{-1} in DPBS (Thermo Fisher Scientific Cat#: 14190-144) with 3 µl of HsPCDH10$_{EC1}$–Fc protein at 3.0 mg ml^{-1}, then immediately

1013   applied 3 µl of sample to glow-discharged Quantifoil grids (R 0.6/1 300 mesh, gold, EMS Cat#:

1014   Q350AR-06) and blotted once for 5 s after a wait time of 15 s in 100% humidity at 4 °C and

1015   plunged into liquid ethane using an FEI Vitrobot Mark IV (Thermo Fisher Scientific). WEEV

1016   Imperial 181 VLPs (with structural polyprotein sequence derived from strain Imperial 181

1017   [GenBank: GQ287641.1]) were also incubated with PdPCDH10$_{EC1}$–Fc for 4 h, and samples were

1018   frozen on Quantifoil grids (R 2/2 300 mesh, gold, EMS Cat#: Q3100AR2). WEEV McMillan VLPs

1019   (with structural polyprotein sequence derived from strain McMillan [GenBank: DQ393792.1]) were

1020   also incubated with VLDLR$_{LBD}$–Fc, and samples were immediately frozen on Quantifoil grids. We

1021   also applied 3 µl of WEEV CBA87 VLP sample onto glow-discharged Quantifoil grids and plunged

1022   into liquid ethane to prepare cryo-EM samples with same parameters as WEEV VLP:PCDH10$_{EC1}$–

1023   Fc complex using an FEI Vitrobot Mark IV. The Cryo-EM data collections were performed using

1024   a 300 kV FEI Titan Krios microscope (Thermo Fisher Scientific) with K3 (Gatan) or Falcon 4

1025   (Thermo Fisher Scientific) direct electron detector at the Harvard Cryo-Electron Microscopy

1026   Center. Automated single-particle data acquisition was performed with SerialEM or EPU, with a

1027   magnification of ×81,000 (K3) or ×130,000 (Falcon 4) in counting mode, which yielded a calibrated

1028   pixel size of 1.06 Å (K3) or 0.94 Å (Falcon 4) and the datasets were collected at defocus ranges

1029   of −0.6 to −1.8 µm or −0.8 to −1.8 µm.

1030

1031   **Cryo-EM data processing**

1032   Raw movie stacks were corrected for beam-induced motion using MotionCor2 (version 1.6.4).[60]

1033   The parameters of the contrast transfer function (CTF) for all micrographs were estimated by

1034   CTFDIND-4.1 (version 4.1.14).[61] For the WEEV CBA87 VLP in complex with HsPCDH10$_{EC1}$–Fc,

1035   a total 22,075 particles were auto-picked from 7,749 micrographs using crYOLO (version 1.8.2),[58]

1036   and particles were extracted with binned two times (pixel size 2.12 Å) in RELION 3.1 (version

1037   3.1.4).[57] After several rounds of reference-free 2D classification, 19,527 particles were selected

1038   from good 2D classes and subjected to 3D classification with icosahedral symmetry, and these

1039   particles were classified into five classes using the 12 Å density map of WEEV VLP (EMD-5210)[68]

1040   as the initial reference model. After 3D classification, a total of 13,141 particles were selected and

1041   subjected to further 3D auto-refinement with icosahedral symmetry, finally yielding 4.8 Å

1042   reconstruction of the WEEV CBA87 VLP:HsPCDH10$_{EC1}$–Fc complex. To improve the resolution

1043   of the map, we used the block-based reconstruction method[69] centered on the q3 spikes. 788,460

1044   blocks were extracted and subjected to 3D classifications without alignment. 343,889 particles

1045   were selected for initial refinement with C1 symmetry, which was followed by CTF refinement,

1046   and a final round of refinement that generated a 3.3 Å map of the q3 spikes. We then used masked

1047   refinement to obtain a 2.9 Å density map of the spike trimer, which includes three copies of E2–

1048   E1 heterodimers and three copies of the capsid. This map was processed using DeepEMhancer

1049   (version 20210511)[59] for cryo-EM volume post-processing to generate a map for model building.

1050   The cryo-EM WEEV VLP alone data were processed with similar data processing

1051   procedure using RELION 3.1 (version 3.1.4),[57] which generated a 5.4 Å map of the WEEV CBA87

1052   VLP alone. Then we got a 3.4 Å map of the q3 spikes by block-based reconstruction method.[69]

1053   This map was processed using DeepEMhancer (version 20210511)[59] for cryo-EM volume post-

1054   processing to generate a map for model building. And the cryo-EM WEEV Imperial 181 VLP

1055   bound to PdPCDH10$_{EC1}$–Fc data were processed with similar data processing procedure using

1056   RELION 3.1 (version 3.1.4),[57] which generated a 4.8 Å map of the WEEV Imperial 181 VLP bound

1057   to PdPCDH10$_{EC1}$–Fc. We then obtained a 2.8 Å map of the trimeric spikes bound to

1058 PdPCDH10$_{EC1}$–Fc using the block-based reconstruction method.[69]

1059   For the WEEV McMillan VLP in complex with VLDLR$_{LBD}$–Fc, we processed the first dataset

1060   with similar data processing steps and get a 5.9 Å map of the WEEV McMillan VLP:VLDLR$_{LBD}$–

1061   Fc. To improve the quality of density map, we collected a second dataset. The second dataset

1062   was processed separately and generated a 4.8 Å map of the WEEV McMillan VLP:VLDLR$_{LBD}$–

1063   Fc. We then combined VLPs from both datasets after the first round of refinement and subjected

1064   them to refinement. Finally, the resolution of the combined WEEV McMillan VLP:VLDLR$_{LBD}$–Fc

1065 complex map was 4.7 Å. We performed block-based reconstruction of q3 spikes of both datasets

1066 independently. We combined good blocks in the 3D classification results of both datasets and

1067 1,720,156 blocks were used to perform 3D auto-refinement, which generated a 2.9 Å map of the

1068 q3 spikes. To improve features for the LA repeat density, an asymmetric unit masked refinement

1069 was performed. The resolution of masked refinement map is 2.8 Å, and DeepEMhancer-post-

1070 processing yielded a density map for model building with details of the spike protein, capsid, and

1071 that were well-resolved. Maps were processed using DeepEMhancer (version 20210511)[59] for

1072 cryo-EM volume post-processing.

1073

1074 **Model building**

1075 For the WEEV CBA87 VLP:HsPCDH10$_{EC1}$–Fc, we used coordinates of PCDH10 EC1 from the

1076 crystal structure of human PCDH10 EC1–EC4 (PDB:6VFQ)[14] and of WEEV E2–E1 and capsid

1077 predicted by AlphaFold2[65] as initial models. These models were docked into the DeepEMhancer

1078 post-processed cryo-EM density map using UCSF ChimeraX (version 1.6.1).[62] The atomic model

1079 was then generated through iterative rounds of model building and adjustment in *Coot* (version

1080 0.9.8.91)[63] and refined using real space refinement in Phenix (version 1.21rc1-5127).[64]

1081 The model of the unliganded WEEV CBA87 VLP was generated based on WEEV CBA87

1082 VLP:HsPCDH10$_{EC1}$–Fc model that was docked into the DeepEMhancer post-processed cryo-EM

1083 density map of the unliganded VLP using UCSF ChimeraX. For the WEEV Imperial 181

1084 VLP:PdPCDH10$_{EC1}$–Fc, the structure CBA87 VLP:HsPCDH10$_{EC1}$–Fc as an initial model was fitted

1085 into the DeepEMhancer post-processed cryo-EM map of the q3 spikes for the Imperial 181

1086 complex. The initial coordinates of WEEV McMillan VLP:VLDLR$_{LBD}$–Fc were generated based on

1087 WEEV CBA87 VLP:HsPCDH10$_{EC1}$–Fc model and VLDLR LA1–LA2 structure predicted by

1088 AlphaFold2.[65] These models were docked into the cryo-EM density for the WEEV McMillan:

1089 VLDLR$_{LBD}$-Fc complex using UCSF ChimeraX.

1090   The atomic models for the unliganded WEEV CBA87 VLP, WEEV Imperial 181

1091   VLP:*Pd*PCDH10$_{EC1}$–Fc, WEEV McMillan VLP:VLDLR$_{LBD}$–Fc were generated through iterative

1092   rounds of model building and adjustment with their associated maps in *Coot* (version 0.9.8.91)[63]

1093   and refined using real space refinement in Phenix (version 1.21rc1-5127).[64]   All models were

1094   validated using RCSB PDB and refinement statistics are provided in Table S2. Figures of

1095   structural presenting were made by either UCSF ChimeraX (version 1.6.1)[62] or PyMOL (version

1096   3.0.2) (https://www.pymol.org/pymol). Software used in this project was curated by SBGrid.[70]

1097

1098   **QUANTIFICATION AND STATISTICAL ANALYSIS**

1099   **Statistical analysis**

1100   Data were deemed statistically significant when P values were <0.05 using version 10 of

1101   GraphPad Prism. Experiments were analyzed by one-way or two-way ANOVA with multiple

1102   comparison correction.

1103

1104   **Author contributions**

1105   X.F. produced VLPs, recombinant Fc-fusion proteins, performed biolayer interferometry and

1106   ELISA experiments, determined cryo-EM structures, and built and refined atomic models. W.L.

1107   generated cell lines, RVPs, and recombinant proteins, and performed infectivity studies and

1108   phylogenetic analysis. J.S.P. generated cell lines and RVPs and performed infectivity studies.

1109   J.O., L.V.T., and L.M.M., generated RVPs and performed infectivity studies. C.J.M., H.V., and

1110   T.K.B. produce recombinant Fc-fusion proteins. V.B. and P.Y. helped generate WEEV CBA87

1111   VLPs. J.M.B., S.N., H.U., H.B., S.Y.C. and I.M.C. participated in experimental design and helped

1112   analyze and interpret data. W.M.dS. and S.C.W. performed ancestral sequence reconstruction.

1113   K.S.P. and J.A.P. analyzed and interpreted data. J.A. acquired funding and supervised the

1114   research. X.F., W.L., and J.A. wrote the original draft of the manuscript, and all authors

1115   participated in reviewing and editing the manuscript.

1116

1117 **Acknowledgements**

1129

1130

References

1. Arechiga-Ceballos, N., and Aguilar-Setien, A. (2015). Alphaviral equine encephalomyelitis (Eastern, Western and Venezuelan). Rev Sci Tech *34*, 491-501. 10.20506/rst.34.2.2374.

2. Griffin, D.E. (2013). Alphaviruses. In Fields Virology, D.M. Knipe, and P.M. Howley, eds. (Lippincott Williams & Wilkins), pp. 651-686.

3. Ronca, S.E., Dineley, K.T., and Paessler, S. (2016). Neurological Sequelae Resulting from Encephalitic Alphavirus Infection. Front Microbiol *7*, 959. 10.3389/fmicb.2016.00959.

4. Bergren, N.A., Haller, S., Rossi, S.L., Seymour, R.L., Huang, J., Miller, A.L., Bowen, R.A., Hartman, D.A., Brault, A.C., and Weaver, S.C. (2020). "Submergence" of Western equine encephalitis virus: Evidence of positive selection argues against genetic drift and fitness reductions. PLoS Pathog *16*, e1008102. 10.1371/journal.ppat.1008102.

5. Aviles, G., Bianchi, T.I., Daffner, J.F., and Sabattini, M.S. (1993). [Post-epizootic activity of Western equine encephalitis virus in Argentina]. Rev Argent Microbiol *25*, 88-99.

6. Delfraro, A., Burgueno, A., Morel, N., Gonzalez, G., Garcia, A., Morelli, J., Perez, W., Chiparelli, H., and Arbiza, J. (2011). Fatal human case of Western equine encephalitis, Uruguay. Emerg Infect Dis *17*, 952-954. 10.3201/eid1705.101068.

7. Campos, A.S., Franco, A.C., Godinho, F.M., Huff, R., Candido, D.S., da Cruz Cardoso, J., Hua, X., Claro, I.M., Morais, P., Franceschina, C., et al. (2024). Molecular Epidemiology of Western Equine Encephalitis Virus, South America, 2023-2024. Emerg Infect Dis *30*, 1834-1840. 10.3201/eid3009.240530.

8. Saul, F., Alessandrini, M.V., Maggi, M., Lombardi, F., and Martiren, M.S. (2024). Western equine encephalitis, a report of two cases in pediatric patients. Arch Argent Pediatr, e202410383. 10.5546/aap.2024-10383.eng.

9. Gonzalez Pannia, P., De Lillo, L., Roldan, M., Mino, L., Pruscino, F., Farias, E., and Juarez, X. (2024). Western equine encephalitis: a pediatric case report. Arch Argent Pediatr, e202410392. 10.5546/aap.2024-10392.eng.

10. Li, W., Plante, J.A., Lin, C., Basu, H., Plung, J.S., Fan, X., Boeckers, J.M., Oros, J., Buck, T.K., Anekal, P.V., et al. (2024). Shifts in receptors during submergence of an encephalitic arbovirus. Nature. 10.1038/s41586-024-07740-2.

11. Yang, Y., Zhao, L.X., Li, Z.Q., Wang, S.Y., Xu, Z.S., and Wang, Y.Y. (2024). PCDH10 is a neuronal receptor for western equine encephalitis virus. Cell Res. 10.1038/s41422-024-01031-1.

12. Hoshina, N., Johnson-Venkatesh, E.M., Rally, V.R., Sant, J., Hoshina, M., Seiglie, M.P., and Umemori, H. (2022). ASD/OCD-Linked Protocadherin-10 Regulates Synapse, But Not Axon, Development in the Amygdala and Contributes to Fear- and Anxiety-Related Behaviors. J Neurosci *42*, 4250-4266. 10.1523/JNEUROSCI.1843-21.2022.

13. Tsai, N.P., Wilkerson, J.R., Guo, W., Maksimova, M.A., DeMartino, G.N., Cowan, C.W., and Huber, K.M. (2012). Multiple autism-linked genes mediate synapse elimination via proteasomal degradation of a synaptic scaffold PSD-95. Cell *151*, 1581-1594. 10.1016/j.cell.2012.11.040.

14. Harrison, O.J., Brasch, J., Katsamba, P.S., Ahlsen, G., Noble, A.J., Dan, H., Sampogna, R.V., Potter, C.S., Carragher, B., Honig, B., and Shapiro, L. (2020). Family-wide Structural and Biophysical Analysis of Binding Interactions among Non-clustered delta-Protocadherins. Cell Rep *30*, 2655-2671 e2657. 10.1016/j.celrep.2020.02.003.

15. Basore, K., Kim, A.S., Nelson, C.A., Zhang, R., Smith, B.K., Uranga, C., Vang, L., Cheng, M., Gross, M.L., Smith, J., et al. (2019). Cryo-EM Structure of Chikungunya Virus in Complex with the Mxra8 Receptor. Cell *177*, 1725-1737 e1716. 10.1016/j.cell.2019.04.006.

16. Basore, K., Ma, H., Kafai, N.M., Mackin, S., Kim, A.S., Nelson, C.A., Diamond, M.S., and Fremont, D.H. (2021). Structure of Venezuelan equine encephalitis virus in complex with the LDLRAD3 receptor. Nature *598*, 672-676. 10.1038/s41586-021-03963-9.

17. Ma, B., Huang, C., Ma, J., Xiang, Y., and Zhang, X. (2021). Structure of Venezuelan equine encephalitis virus with its receptor LDLRAD3. Nature *598*, 677-681. 10.1038/s41586-021-03909-1.

18. Song, H., Zhao, Z., Chai, Y., Jin, X., Li, C., Yuan, F., Liu, S., Gao, Z., Wang, H., Song, J., et al. (2019). Molecular Basis of Arthritogenic Alphavirus Receptor MXRA8 Binding to Chikungunya Virus Envelope Protein. Cell *177*, 1714-1724 e1712. 10.1016/j.cell.2019.04.008.

19. Yang, P., Li, W., Fan, X., Pan, J., Mann, C.J., Varnum, H., Clark, L.E., Clark, S.A., Coscia, A., Basu, H., et al. (2024). Structural basis for VLDLR recognition by eastern equine encephalitis virus. Nat Commun *15*, 6548. 10.1038/s41467-024-50887-9.

20. Adams, L.J., Raju, S., Ma, H., Gilliland, T., Jr., Reed, D.S., Klimstra, W.B., Fremont, D.H., and Diamond, M.S. (2024). Structural and functional basis of VLDLR usage by Eastern equine encephalitis virus. Cell *187*, 360-374 e319. 10.1016/j.cell.2023.11.031.

21. Cao, D., Ma, B., Cao, Z., Xu, X., Zhang, X., and Xiang, Y. (2024). The receptor VLDLR binds Eastern Equine Encephalitis virus through multiple distinct modes. Nat Commun *15*, 6866. 10.1038/s41467-024-51293-x.

22. Cao, D., Ma, B., Cao, Z., Zhang, X., and Xiang, Y. (2023). Structure of Semliki Forest virus in complex with its receptor VLDLR. Cell *186*, 2208-2218 e2215. 10.1016/j.cell.2023.03.032.

23. Palakurty, S., Raju, S., Sariol, A., Chong, Z., Wagoner, N., Ma, H., Zimmerman, O., Adams, L.J., Carmona, C., Liu, Z., et al. (2024). The VLDLR entry receptor is required for the pathogenesis of multiple encephalitic alphaviruses. Cell Rep *43*, 114809. 10.1016/j.celrep.2024.114809.

24. Logue, C.H., Bosio, C.F., Welte, T., Keene, K.M., Ledermann, J.P., Phillips, A., Sheahan, B.J., Pierro, D.J., Marlenee, N., Brault, A.C., et al. (2009). Virulence variation among isolates of western equine encephalitis virus in an outbred mouse model. J Gen Virol *90*, 1848-1858. 10.1099/vir.0.008656-0.

25. Burton, A.N., McLintock, J., and Rempel, J.G. (1966). Western equine encephalitis virus in Saskatchewan garter snakes and leopard frogs. Science *154*, 1029-1031. 10.1126/science.154.3752.1029.

26. Thomas, L.A., and Eklund, C.M. (1962). Overwintering of western equine encephalomyelitis virus in garter snakes experimentally infected by Culex tarsalis. Proc Soc Exp Biol Med *109*, 421-424. 10.3181/00379727-109-27225.

27. Cheng, R.H., Kuhn, R.J., Olson, N.H., Rossmann, M.G., Choi, H.K., Smith, T.J., and Baker, T.S. (1995). Nucleocapsid and glycoprotein organization in an enveloped virus. Cell *80*, 621-630. 10.1016/0092-8674(95)90516-2.

28. Paredes, A.M., Brown, D.T., Rothnagel, R., Chiu, W., Schoepp, R.J., Johnston, R.E., and Prasad, B.V. (1993). Three-dimensional structure of a membrane-containing virus. Proc Natl Acad Sci U S A *90*, 9095-9099. 10.1073/pnas.90.19.9095.

29. Paredes, A.M., Simon, M.N., and Brown, D.T. (1992). The mass of the Sindbis virus nucleocapsid suggests it has T = 4 icosahedral symmetry. Virology *187*, 329-332. 10.1016/0042-6822(92)90322-g.

30. Ko, S.Y., Akahata, W., Yang, E.S., Kong, W.P., Burke, C.W., Honnold, S.P., Nichols, D.K., Huang, Y.S., Schieber, G.L., Carlton, K., et al. (2019). A virus-like particle vaccine prevents equine encephalitis virus infection in nonhuman primates. Sci Transl Med *11*. 10.1126/scitranslmed.aav3113.

31. Lozzio, C.B., and Lozzio, B.B. (1975). Human chronic myelogenous leukemia cell-line with positive Philadelphia chromosome. Blood *45*, 321-334. 10.1182/blood-2016-08-736025.

32. Fass, D., Blacklow, S., Kim, P.S., and Berger, J.M. (1997). Molecular basis of familial hypercholesterolaemia from structure of LDL receptor module. Nature *388*, 691-693. 10.1038/41798.

33. Fisher, C., Beglova, N., and Blacklow, S.C. (2006). Structure of an LDLR-RAP complex reveals a general mode for ligand recognition by lipoprotein receptors. Mol Cell *22*, 277-283. 10.1016/j.molcel.2006.02.021.

34. Yasui, N., Nogi, T., and Takagi, J. (2010). Structural basis for specific recognition of reelin by its receptors. Structure *18*, 320-331. 10.1016/j.str.2010.01.010.

35. Nikolic, J., Belot, L., Raux, H., Legrand, P., Gaudin, Y., and A, A.A. (2018). Structural basis for the recognition of LDL-receptor family members by VSV glycoprotein. Nat Commun *9*, 1029. 10.1038/s41467-018-03432-4.

36. Verdaguer, N., Fita, I., Reithmayer, M., Moser, R., and Blaas, D. (2004). X-ray structure of a minor group human rhinovirus bound to a fragment of its cellular receptor protein. Nat Struct Mol Biol *11*, 429-434. 10.1038/nsmb753.

37. Li, Y., Zhao, Z., Liu, S., Wang, H., Sun, J., Chai, Y., Zhou, J., Wang, Y., Shi, Y., Song, H., and Gao, G.F. (2023). Structural basis of Semliki Forest virus entry using the very-low-density lipoprotein receptor. hLife *1*, 124-136. 10.1016/j.hlife.2023.11.001.

38. Mossel, E.C., Ledermann, J.P., Phillips, A.T., Borland, E.M., Powers, A.M., and Olson, K.E. (2013). Molecular determinants of mouse neurovirulence and mosquito infection for Western equine encephalitis virus. PLoS One *8*, e60427. 10.1371/journal.pone.0060427.

39. Clark, L.E., Clark, S.A., Lin, C., Liu, J., Coscia, A., Nabel, K.G., Yang, P., Neel, D.V., Lee, H., Brusic, V., et al. (2022). VLDLR and ApoER2 are receptors for multiple alphaviruses. Nature *602*, 475-480. 10.1038/s41586-021-04326-0.

40. Mitchell, C.J., Monath, T.P., Sabattini, M.S., Cropp, C.B., Daffner, J.F., Calisher, C.H., Jakob, W.L., and Christensen, H.A. (1985). Arbovirus investigations in Argentina, 1977-1980. II. Arthropod collections and virus isolations from Argentine mosquitoes. Am J Trop Med Hyg *34*, 945-955.

41. Zimmerman, O., Zimmerman, M.I., Raju, S., Nelson, C.A., Errico, J.M., Madden, E.A., Holmes, A.C., Hassan, A.O., VanBlargan, L.A., Kim, A.S., et al. (2023). Vertebrate-class-specific binding modes of the alphavirus receptor MXRA8. Cell *186*, 4818-4833 e4825. 10.1016/j.cell.2023.09.007.

42. Allison, A.B., and Stallknecht, D.E. (2009). Genomic sequencing of Highlands J virus: a comparison to western and eastern equine encephalitis viruses. Virus Res *145*, 334-340. 10.1016/j.virusres.2009.07.016.

43. Ip, H.S., Wiley, M.R., Long, R., Palacios, G., Shearn-Bochsler, V., and Whitehouse, C.A. (2014). Identification and characterization of Highlands J virus from a Mississippi sandhill crane using unbiased next-generation sequencing. J Virol Methods *206*, 42-45. 10.1016/j.jviromet.2014.05.018.

44. Eleazer, T.H., and Hill, J.E. (1994). Highlands J virus-associated mortality in chukar partridges. J Vet Diagn Invest *6*, 98-99. 10.1177/104063879400600118.

45. Ficken, M.D., Wages, D.P., Guy, J.S., Quinn, J.A., and Emory, W.H. (1993). High mortality of domestic turkeys associated with Highlands J virus and eastern equine encephalitis virus infections. Avian Dis *37*, 585-590.

46. Meehan, P.J., Wells, D.L., Paul, W., Buff, E., Lewis, A., Muth, D., Hopkins, R., Karabatsos, N., and Tsai, T.F. (2000). Epidemiological features of and public health response to a St. Louis encephalitis epidemic in Florida, 1990-1. Epidemiol Infect *125*, 181-188. 10.1017/s0950268899004227.

47. Karabatsos, N., Lewis, A.L., Calisher, C.H., Hunt, A.R., and Roehrig, J.T. (1988). Identification of Highlands J virus from a Florida horse. Am J Trop Med Hyg *39*, 603-606. 10.4269/ajtmh.1988.39.603.

48. Bergren, N.A., Auguste, A.J., Forrester, N.L., Negi, S.S., Braun, W.A., and Weaver, S.C. (2014). Western equine encephalitis virus: evolutionary analysis of a declining alphavirus based on complete genome sequences. J Virol *88*, 9260-9267. 10.1128/JVI.01463-14.

49. Gardner, C.L., Sun, C., Dunn, M.D., Gilliland, T.C., Jr., Trobaugh, D.W., Terada, Y., Reed, D.S., Hartman, A.L., and Klimstra, W.B. (2022). In Vitro and In Vivo Phenotypes of

Venezuelan, Eastern and Western Equine Encephalitis Viruses Derived from cDNA Clones of Human Isolates. Viruses *15*. 10.3390/v15010005.

50. Pauvolid-Correa, A., Juliano, R.S., Campos, Z., Velez, J., Nogueira, R.M., and Komar, N. (2015). Neutralising antibodies for Mayaro virus in Pantanal, Brazil. Mem Inst Oswaldo Cruz *110*, 125-133. 10.1590/0074-02760140383.

51. Pauvolid-Correa, A., Tavares, F.N., Costa, E.V., Burlandy, F.M., Murta, M., Pellegrin, A.O., Nogueira, M.F., and Silva, E.E. (2010). Serologic evidence of the recent circulation of Saint Louis encephalitis virus and high prevalence of equine encephalitis viruses in horses in the Nhecolandia sub-region in South Pantanal, Central-West Brazil. Mem Inst Oswaldo Cruz *105*, 829-833. 10.1590/s0074-02762010000600017.

52. Nunes, J., Casseb, L.M.N., Guimaraes, R., Reis, W.D.M., de Barros, B.C.V., Ferreira, M.S., Chiang, J.O., Pinheiro, H.H.C., Vasconcelos, P., and Cruz, A.C.R. (2021). Serological evidence of Eastern equine encephalitis circulation in equids in Para state, Brazil. Braz J Vet Med *43*, e001720. 10.29374/2527-2179.bjvm001720.

53. Sun, Y., Watters, K., Hill, M.G., Fang, Q., Liu, Y., Kuhn, R.J., Klose, T., Rossmann, M.G., and Palmenberg, A.C. (2020). Cryo-EM structure of rhinovirus C15a bound to its cadherin-related protein 3 receptor. Proc Natl Acad Sci U S A *117*, 6784-6791. 10.1073/pnas.1921640117.

54. Robert, X., and Gouet, P. (2014). Deciphering key features in protein structures with the new ENDscript server. Nucleic Acids Res *42*, W320-324. 10.1093/nar/gku316.

55. Voss, J.E., Vaney, M.C., Duquerroy, S., Vonrhein, C., Girard-Blanc, C., Crublet, E., Thompson, A., Bricogne, G., and Rey, F.A. (2010). Glycoprotein organization of Chikungunya virus particles revealed by X-ray crystallography. Nature *468*, 709-712. 10.1038/nature09555.

56. Sutton, M.S., Pletnev, S., Callahan, V., Ko, S., Tsybovsky, Y., Bylund, T., Casner, R.G., Cerutti, G., Gardner, C.L., Guirguis, V., et al. (2023). Vaccine elicitation and structural basis for antibody protection against alphaviruses. Cell *186*, 2672-2689 e2625. 10.1016/j.cell.2023.05.019.

57. Zivanov, J., Nakane, T., Forsberg, B.O., Kimanius, D., Hagen, W.J., Lindahl, E., and Scheres, S.H. (2018). New tools for automated high-resolution cryo-EM structure determination in RELION-3. Elife *7*. 10.7554/eLife.42166.

58. Wagner, T., Merino, F., Stabrin, M., Moriya, T., Antoni, C., Apelbaum, A., Hagel, P., Sitsel, O., Raisch, T., Prumbaum, D., et al. (2019). SPHIRE-crYOLO is a fast and accurate fully automated particle picker for cryo-EM. Commun Biol *2*, 218. 10.1038/s42003-019-0437-z.

59. Sanchez-Garcia, R., Gomez-Blanco, J., Cuervo, A., Carazo, J.M., Sorzano, C.O.S., and Vargas, J. (2021). DeepEMhancer: a deep learning solution for cryo-EM volume post-processing. Commun Biol *4*, 874. 10.1038/s42003-021-02399-1.

60. Zheng, S.Q., Palovcak, E., Armache, J.P., Verba, K.A., Cheng, Y., and Agard, D.A. (2017). MotionCor2: anisotropic correction of beam-induced motion for improved cryo-electron microscopy. Nat Methods *14*, 331-332. 10.1038/nmeth.4193.

61. Rohou, A., and Grigorieff, N. (2015). CTFFIND4: Fast and accurate defocus estimation from electron micrographs. J Struct Biol *192*, 216-221. 10.1016/j.jsb.2015.08.008.

62. Pettersen, E.F., Goddard, T.D., Huang, C.C., Couch, G.S., Greenblatt, D.M., Meng, E.C., and Ferrin, T.E. (2004). UCSF Chimera--a visualization system for exploratory research and analysis. J Comput Chem *25*, 1605-1612. 10.1002/jcc.20084.

63. Emsley, P., Lohkamp, B., Scott, W.G., and Cowtan, K. (2010). Features and development of Coot. Acta Crystallogr D Biol Crystallogr *66*, 486-501. 10.1107/S0907444910007493.

64. Adams, P.D., Afonine, P.V., Bunkoczi, G., Chen, V.B., Davis, I.W., Echols, N., Headd, J.J., Hung, L.W., Kapral, G.J., Grosse-Kunstleve, R.W., et al. (2010). PHENIX: a comprehensive Python-based system for macromolecular structure solution. Acta Crystallogr D Biol Crystallogr *66*, 213-221. 10.1107/S0907444909052925.

65. Jumper, J., Evans, R., Pritzel, A., Green, T., Figurnov, M., Ronneberger, O., Tunyasuvunakool, K., Bates, R., Zidek, A., Potapenko, A., et al. (2021). Highly accurate protein structure prediction with AlphaFold. Nature *596*, 583-589. 10.1038/s41586-021-03819-2.

66. Bajic, G., Maron, M.J., Adachi, Y., Onodera, T., McCarthy, K.R., McGee, C.E., Sempowski, G.D., Takahashi, Y., Kelsoe, G., Kuraoka, M., and Schmidt, A.G. (2019). Influenza antigen engineering focuses immune responses to a subdominant but broadly protective viral epitope. Cell Host Microbe *25*, 827-835 e826. 10.1016/j.chom.2019.04.003.

67. Kuhn, R.J., Niesters, H.G., Hong, Z., and Strauss, J.H. (1991). Infectious RNA transcripts from Ross River virus cDNA clones and the construction and characterization of defined chimeras with Sindbis virus. Virology *182*, 430-441. 10.1016/0042-6822(91)90584-x.

68. Sherman, M.B., and Weaver, S.C. (2010). Structure of the Recombinant Alphavirus Western Equine Encephalitis Virus Revealed by Cryoelectron Microscopy. Journal of Virology *84*, 9775-9782. doi:10.1128/jvi.00876-10.

69. Zhu, D., Wang, X., Fang, Q., Van Etten, J.L., Rossmann, M.G., Rao, Z., and Zhang, X. (2018). Pushing the resolution limit by correcting the Ewald sphere effect in single-particle Cryo-EM reconstructions. Nat Commun *9*, 1552. 10.1038/s41467-018-04051-9.

70. Morin, A., Eisenbraun, B., Key, J., Sanschagrin, P.C., Timony, M.A., Ottaviano, M., and Sliz, P. (2013). Collaboration gets the most out of software. Elife *2*, e01456. 10.7554/eLife.01456.